Phase separation of signaling molecules promotes T cell receptor signal transduction

Authors: Xiaolei Su[1,2,*], Jonathon A. Ditlev[1,3,*], Enfu Hui[1,2], Wenmin Xing[1,3], Sudeep Banjade[1,3], Julia Okrut[1,2], David S. King[4], Jack Taunton[1,2], Michael K. Rosen[1,3,‡], and Ronald D. Vale[1,2,‡]

Affiliations:

[1]The HHMI Summer Institute, Marine Biological Laboratory, Woods Hole, MA 02543, USA.

[2]Department of Cellular and Molecular Pharmacology and Howard Hughes Medical Institute, University of California, San Francisco, CA 94158, USA.

[3]Department of Biophysics and Howard Hughes Medical Institute, University of Texas Southwestern Medical Center, Dallas, TX 75390, USA.

[4]Howard Hughes Medical Institute Mass Spectrometry Laboratory and Department of Molecular and Cellular Biology, University of California, Berkeley, CA 94720, USA.

[‡]Corresponding author. E-mail: ron.vale@ucsf.edu (R.D.V.); michael.rosen@utsouthwestern.edu (M.K.R.)

[*]These authors contributed equally to this work.

Abstract

Activation of various cell surface receptors triggers the reorganization of downstream signaling molecules into micron- or submicron-sized clusters. However, the functional consequences of such clustering has been unclear. We biochemically reconstituted a 12-component signaling pathway on model membranes, beginning with T cell receptor (TCR) activation and ending with actin assembly. When TCR phoshophorylation was triggered, downstream signaling proteins spontaneously separated into liquid-like clusters that promoted signaling outputs both in vitro and in human Jurkat T cells. Reconstituted clusters were enriched in kinases but excluded phosphatases, and enhanced actin filament assembly by recruiting and organizing actin regulators. These results demonstrate that protein phase separation can create a distinct physical and biochemical compartment that facilitates signaling.

One Sentence Summary: Reconstitution of a T cell signaling pathway and correlative cellular studies reveal how phase separation of molecules into microclusters can promote biochemical reactions and signaling responses.

Main Text

Many cell surface receptors and downstream signaling molecules coalesce into micron- or submicron-sized clusters upon initiation of signaling (*1, 2*). However, the effect of this clustering on signal transduction is poorly understood. T cell receptor (TCR) signaling is a well-studied example of this general phenomenon (*3*). TCR signaling proceeds through a series of biochemical reactions that can be viewed as connected modules. In the upstream module, the TCR is phosphorylated by Lck, a membrane-bound protein kinase of the Src family. TCR phosphorylation is opposed by a transmembrane phosphatase, CD45 (*3*). The phosphorylated cytoplasmic domains of the TCR complex recruit and activate the cytosolic tyrosine kinase ZAP70 (*4*). In the intermediate module, ZAP70 phosphorylates the transmembrane protein LAT (Linker for activation of T cells) on multiple tyrosine residues. These phosphotyrosines are binding sites for adapter proteins Grb2 and Gads, which further interact with Sos1 (a guanine nucleotide exchange factor (GEF) for the small guanosine triphosphatase Ras) or SLP-76 (another adaptor in TCR signaling). Components of the LAT complex activate several downstream modules that mediate calcium mobilization, mitogen-activated protein kinase (MAPK) activation, and actin polymerization (*5, 6*).

LAT and its binding partners coalesce into micron- or submicron-sized clusters at the plasma membrane upon TCR activation (*7-10*). Elimination of these microclusters by deletion of key components (for example, LAT or Grb2) impairs downstream signaling and transcriptional responses (*5, 11*). However, effects due to loss of clusters have not been distinguished from those due to loss of component molecules. Nor do we understand the changes in biochemistry and consequent signaling that emerge specifically when signaling molecules are organized from an unclustered to a clustered state (*12*).

To explore the mechanism of formation and functional consequences of T cell microclusters, we reconstituted a TCR signaling pathway from purified components. To substitute for the plasma membrane, we used supported bilayers composed of a defined, simple lipid composition. We initially reconstituted the intermediate module of the TCR signaling cascade, composed of phosphorylated LAT (pLAT), Grb2, and Sos1. Multivalent interactions between these proteins (Fig. 1A) are thought to drive the formation of signaling microclusters on the T cell membrane (*8, 13*), although direct experimental evidence for the sufficiency of this mechanism has been lacking. We prepared fluorescently labeled pLAT, containing the four C-terminal phospho-tyrosine residues that are sufficient for TCR signaling (*14*); this pLAT also contains an N-terminal His_8 tag that allowed its attachment to Ni^{2+}-containing supported lipid bilayers (*15*). pLAT was uniformly distributed (Fig. 1B) and freely diffused on the lipid bilayer (movie S1). Upon addition of Grb2 and Sos1, submicron-sized clusters formed within 1 minute and gradually grew in size. Cluster formation required tyrosine phosphorylation of LAT (fig. S1D). Furthermore, dephosphorylation of pLAT by high concentrations of the soluble protein tyrosine phosphatase 1B (PTP1B, 2 μM) caused the clusters to disassemble (Fig. 1B, movie S2). pLAT, Grb2, and Sos1 all colocalized within clusters, and clusters did not form if either Grb2 or Sos1 was omitted (fig. S1E, F). pLAT also clustered with Gads and SLP-76, two other components of LAT clusters in cells (*6, 7*), but less efficiently than with Grb2 and Sos1 (fig. S2A, B). Clustering efficiency, however, increased dramatically with the addition of Nck (fig. S2C), an adaptor protein known to link SLP-76 to actin regulators (*16*).

pLAT, Grb2, and Sos1 clusters exhibited dynamic liquid-like properties. The rounded edges of clusters fluctuated (extending and retracting) on a time scale of seconds and clusters sometimes fused with one another (movie S2). pLAT molecules exchanged into and out of

clusters, as revealed by fluorescence recovery after photobleaching (FRAP) (Fig. 1C). Single pLAT molecules diffused rapidly outside of clusters but slowly within them (fig. S3A-C). We also observed capture and release of single molecules by clusters (movie S3). These results show that pLAT microclusters are liquid-like, phase-separated structures (*17, 18*) on membranes.

Both SH3 domains of Grb2 were required for cluster formation, indicating a role of protein cross-bridging by this adaptor protein (Fig. 1D and fig. S4A). Clustering initially increased with increasing pLAT density but then decreased at higher pLAT densities on the membrane (fig. S4B), consistent with a theoretical multivalent interaction model (*19*). The valency of phospho-tyrosines on LAT also affected clustering efficiency. Three of the four distal phospho-tyrosines in LAT are recognized by the SH2 domain of Grb2 (*20*). Clustering in vitro progressively decreased by mutating one, two, or all three tyrosines and was enhanced by doubling the number of tyrosines (Fig. 1E and fig. S5). Together, our data indicate that LAT cluster formation is driven by dynamically rearranging, multivalent protein-protein interactions.

We compared the properties of LAT clusters in cells with those of reconstituted clusters in vitro and tested their functional importance. As in vitro, LAT microclusters in T cells sometimes fused with one another (fig. S3D). FRAP revealed that molecules exchange into and out of clusters in cells faster than in vitro ($t_{1/2}$ of 12 sec versus 76 sec), possibly due to different cluster size (see Supplementary Text) or membrane fluidity. To assess valency dependence in cells, we expressed LAT tyrosine mutants with zero, one, two, three, or six Grb2 binding sites in a LAT-deficient Jurkat T cell line. A minimum of two Grb2 binding sites was required for robust cluster formation and the degree of clustering increased with increasing number of phospho-tyrosine sites (Fig. 2B). The degree of clustering correlated with activation of MAPK(ERK) (Fig. 2C), suggesting that clustering of LAT and its partners is important for TCR signaling.

We used our in vitro assay to gain insight into the biochemical reactions that underlie the TCR signaling pathway. To LAT and its binding partners, we introduced the upstream signaling module consisting of: i) the cytoplasmic domain of the TCR subunit CD3ζ (which is sufficient to induce signaling in T cells (*21*)), ii) Lck, which phosphorylates the TCR, iii) the cytoplasmic domain of the tyrosine phosphatase CD45, which opposes this reaction (*22*), and iv) the protein kinase ZAP70, which is recruited to the phosphorylated TCR and phosphorylates LAT (*4, 5*) (Fig. 3A). Initially, unphosphorylated LAT was evenly distributed on the membrane. After ATP was added to initiate Lck phosphorylation of CD3ζ, ZAP70 was recruited to the membrane and LAT clustered (Fig. 3B; fig. S6A). ZAP70 was enriched in the clusters, as observed in T cells (*7*), whereas CD45 was excluded (Fig. 3B). The exclusion of CD45 was recapitulated in a simpler system in which clusters were formed by pLAT, Grb2, and Sos1 (Fig. 3C). The cytoplasmic domain of CD45 has a negative charge (pI 6.4). Assays with a series of differentially charged proteins revealed that, in general, positive charge favors inclusion into and negative charge favors exclusion from LAT clusters (fig. S7 and Supplementary Text). Consistent with limited access of CD45 to pLAT in the cluster center, CD45-mediated dephosphorylation of pLAT was reduced compared to that in unclustered conditions (Fig. 3D). In summary, our data demonstrate that LAT clusters are depleted in the phosphatase CD45 but enriched in the kinase ZAP70, which would be expected to promote LAT phosphorylation and increase the strength of TCR signaling.

We sought to integrate a downstream module that controls an important signaling output, actin polymerization (*23, 24*). We attached His-tagged Lck, CD3ζ, and unphosphorylated LAT-Alexa647 to the supported lipid bilayer and added soluble ZAP70-505-Star, Gads, SLP-76, Nck, N-WASp (neuronal Wiskott-Aldrich Syndrome protein), Arp2/3 (Actin-related protein 2 and 3)

complex, and rhodamine-labeled monomeric actin to the solution (Fig. 4A). Previous data have shown that Nck recruits N-WASp, which in turn activates the Arp2/3 complex to nucleate actin filaments (*16, 25*). When ATP was added to initiate TCR phosphorylation, ZAP70 was recruited to the membrane, followed by LAT clustering and then actin polymerization from the LAT clusters (Fig. 4B,C and fig. S8). Later, when actin bundles formed, LAT clusters became rod-like and aligned with actin bundles (Fig. 4D and movie S4,5). This shape change is reversible, as clusters became round following depolymerization of F-actin by Latrunculin A (fig. S9C). In summary, we show that actin polymerization is initiated from and can reorganize LAT clusters.

We next tested if clustering of Nck affects the efficiency of actin polymerization. In principle, actin polymerization could be stimulated by i) recruitment of Nck from solution to the membrane, ii) concentration and organization of Nck within clusters, or iii) both effects. To isolate spatial distribution as a variable, we attached His_{10}-Nck to Ni-modified lipids in the planar bilayer, and added soluble N-WASp, Arp2/3 complex, and actin. Increasing the density of Nck on the membrane resulted in a dose-dependent increase in assembly of actin (fig. S10). Using a density of Nck (150 molecules/μm^2) at which little actin polymerized, we tested whether clustering of Nck by pLAT, Gads, and pSLP-76 affected actin assembly. Clustering of Nck enhanced total actin assembly on the membrane by 6-fold (Fig. 4E). These results reveal that the clustering of actin regulators by LAT promotes actin polymerization beyond what can be achieved by recruitment to the membrane.

In summary, we reconstituted biochemical reactions of TCR signaling in an in vitro system, in which the components and their concentrations in the reaction can be controlled, rates can be measured, and molecular behaviors can be observed in ways that are difficult to achieve using intact cells. We observed multivalent assembly and consequent phase separation of LAT and its

binding partners into liquid-like, micron-sized clusters. By manipulating clustering using LAT phosphorylation mutants, we show that clustering occurs through analogous mechanisms in vitro and in cells, and that clustering promotes MAPK(ERK) signaling. Thus, as in three-dimensional phase separation (*17, 26*), our results demonstrate that phase separation on membranes can create an environment that promotes biochemical reactions. LAT clusters excluded CD45 and retained ZAP70 to create an environment that perpetuated the phosphorylated state of LAT. Clustering of LAT promoted downstream biochemical reactions in the signaling pathway, specifically the ability of Nck to promote N-WASp-Arp2/3 mediated actin polymerization (fig. S11), as suggested by Nck density-dependent actin polymerization in cells (*27*). Multivalent interactions have been proposed to drive the assembly of many other cellular structures, including PML bodies, stress granules, and focal adhesions (*17, 26*), thus the mechanisms of spatial organization of biochemical reactions revealed here may apply to other cellular processes as well.

References and Notes

1. H. Wu, Higher-order assemblies in a new paradigm of signal transduction. *Cell* **153**, 287-292 (2013).
2. M. Bienz, Signalosome assembly by domains undergoing dynamic head-to-tail polymerization. *Trends in biochemical sciences* **39**, 487-495 (2014).
3. A. K. Chakraborty, A. Weiss, Insights into the initiation of TCR signaling. *Nature immunology* **15**, 798-807 (2014).
4. A. C. Chan, M. Iwashima, C. W. Turck, A. Weiss, ZAP-70: a 70 kd protein-tyrosine kinase that associates with the TCR zeta chain. *Cell* **71**, 649-662 (1992).
5. W. Zhang, J. Sloan-Lancaster, J. Kitchen, R. P. Trible, L. E. Samelson, LAT: the ZAP-70 tyrosine kinase substrate that links T cell receptor to cellular activation. *Cell* **92**, 83-92 (1998).
6. R. T. Abraham, A. Weiss, Jurkat T cells and development of the T-cell receptor signalling paradigm. *Nature reviews. Immunology* **4**, 301-308 (2004).
7. S. C. Bunnell, D. I. Hong, J. R. Kardon, T. Yamazaki, C. J. McGlade, V. A. Barr, L. E. Samelson, T cell receptor ligation induces the formation of dynamically regulated signaling assemblies. *The Journal of cell biology* **158**, 1263-1275 (2002).
8. A. D. Douglass, R. D. Vale, Single-molecule microscopy reveals plasma membrane microdomains created by protein-protein networks that exclude or trap signaling molecules in T cells. *Cell* **121**, 937-950 (2005).
9. R. Varma, G. Campi, T. Yokosuka, T. Saito, M. L. Dustin, T cell receptor-proximal signals are sustained in peripheral microclusters and terminated in the central supramolecular activation cluster. *Immunity* **25**, 117-127 (2006).
10. K. L. Singleton, K. T. Roybal, Y. Sun, G. Fu, N. R. Gascoigne, N. S. van Oers, C. Wulfing, Spatiotemporal patterning during T cell activation is highly diverse. *Science signaling* **2**, ra15 (2009).
11. M. Y. Bilal, J. C. Houtman, GRB2 Nucleates T Cell Receptor-Mediated LAT Clusters That Control PLC-gamma1 Activation and Cytokine Production. *Frontiers in immunology* **6**, 141 (2015).
12. M. L. Dustin, J. T. Groves, Receptor signaling clusters in the immune synapse. *Annual review of biophysics* **41**, 543-556 (2012).

13. J. C. Houtman, H. Yamaguchi, M. Barda-Saad, A. Braiman, B. Bowden, E. Appella, P. Schuck, L. E. Samelson, Oligomerization of signaling complexes by the multipoint binding of GRB2 to both LAT and SOS1. *Nature structural & molecular biology* **13**, 798-805 (2006).

14. M. Zhu, E. Janssen, W. Zhang, Minimal requirement of tyrosine residues of linker for activation of T cells in TCR signaling and thymocyte development. *Journal of immunology* **170**, 325-333 (2003).

15. Materials and methods are available as supplementary materials on Science Online.

16. L. Wunderlich, A. Farago, J. Downward, L. Buday, Association of Nck with tyrosine-phosphorylated SLP-76 in activated T lymphocytes. *European journal of immunology* **29**, 1068-1075 (1999).

17. P. Li, S. Banjade, H. C. Cheng, S. Kim, B. Chen, L. Guo, M. Llaguno, J. V. Hollingsworth, D. S. King, S. F. Banani, P. S. Russo, Q. X. Jiang, B. T. Nixon, M. K. Rosen, Phase transitions in the assembly of multivalent signalling proteins. *Nature* **483**, 336-340 (2012).

18. S. Banjade, M. K. Rosen, Phase transitions of multivalent proteins can promote clustering of membrane receptors. *eLife* **3**, (2014).

19. A. Nag, M. I. Monine, J. R. Faeder, B. Goldstein, Aggregation of membrane proteins by cytosolic cross-linkers: theory and simulation of the LAT-Grb2-SOS1 system. *Biophysical journal* **96**, 2604-2623 (2009).

20. M. Tinti, L. Kiemer, S. Costa, M. L. Miller, F. Sacco, J. V. Olsen, M. Carducci, S. Paoluzi, F. Langone, C. T. Workman, N. Blom, K. Machida, C. M. Thompson, M. Schutkowski, S. Brunak, M. Mann, B. J. Mayer, L. Castagnoli, G. Cesareni, The SH2 domain interaction landscape. *Cell reports* **3**, 1293-1305 (2013).

21. B. A. Irving, A. Weiss, The cytoplasmic domain of the T cell receptor zeta chain is sufficient to couple to receptor-associated signal transduction pathways. *Cell* **64**, 891-901 (1991).

22. E. Hui, R. D. Vale, In vitro membrane reconstitution of the T-cell receptor proximal signaling network. *Nature structural & molecular biology* **21**, 133-142 (2014).

23. S. Kumari, D. Depoil, R. Martinelli, E. Judokusumo, G. Carmona, F. B. Gertler, L. C. Kam, C. V. Carman, J. K. Burkhardt, D. J. Irvine, M. L. Dustin, Actin foci facilitate activation of the phospholipase C-gamma in primary T lymphocytes via the WASP pathway. *eLife* **4**, (2015).

24. S. C. Bunnell, V. Kapoor, R. P. Trible, W. Zhang, L. E. Samelson, Dynamic actin polymerization drives T cell receptor-induced spreading: a role for the signal transduction adaptor LAT. *Immunity* **14**, 315-329 (2001).

25. R. Rohatgi, P. Nollau, H. Y. Ho, M. W. Kirschner, B. J. Mayer, Nck and phosphatidylinositol 4,5-bisphosphate synergistically activate actin polymerization through the N-WASP-Arp2/3 pathway. *The Journal of biological chemistry* **276**, 26448-26452 (2001).

26. A. A. Hyman, C. A. Weber, F. Julicher, Liquid-liquid phase separation in biology. *Annual review of cell and developmental biology* **30**, 39-58 (2014).

27. J. A. Ditlev, P. J. Michalski, G. Huber, G. M. Rivera, W. A. Mohler, L. M. Loew, B. J. Mayer, Stoichiometry of Nck-dependent actin polymerization in living cells. *The Journal of cell biology* **197**, 643-658 (2012).

Acknowledgements

We thank Steve Ross and Lynne Chang at Nikon Instruments for their loan of TIRF-capable microscopes, Nico Stuurman for help with microscopy, Art Weiss for providing JCam2.5 cells, David Liu for providing charged GFP constructs, Chi Pak for providing charged GFP proteins, James Muller for providing ICAM-1 protein, and Luke Rice, Xing Zeng, and members from the Vale Laboratory for comments on this manuscript. This work was supported by the HCIA program of HHMI, the NIH (R01-GM56322 to M.K.R.) and Welch Foundation (I–1544 to M.K.R.). X.S. was supported by CRI Irvington postdoctoral fellowship. J.A.D. was supported by NRSA F32 award 5-F32-DK101188. E.H. was supported as a fellow of the Leukemia and Lymphoma Society. J.O. was supported by funds from Tobacco-Related Disease Research Program of the University of California (19FT-0090).

Supplementary Materials

www.sciencemag.org

Fig. 1. **Multivalent interactions drive LAT cluster formation.**

(A) Schematic of the proteins and interactions in the clustering assay. **(B)** Total internal reflection fluorescence microscopy (TIRF) imaging of LAT clustering and declustering. Clusters formed after adding Grb2 (0.5 μM) and Sos1 (0.25 μM, the proline-rich motifs) to membrane-bound pLAT-Alexa488 (1000 molecules/μm^2) at 0 min and dissolved after adding the protein tyrosine phosphatase PTP1B (2 μM) at 9 min. Scale bar: 2 μm. See movie S2. **(C)** Fluorescence recovery after photobleaching (FRAP) of clustered pLAT on planar lipid bilayers; time 0 indicates the time of the photobleaching pulse. Bottom plot shows the time course of the recovery of pLAT-Alexa488 (300 molecules/μm^2) formed by 1 μM Grb2 and 2 μM Sos1. Shown are the mean ± s.d. (N=7 pLAT clusters). Scale bar, 2 μm. **(D)** TIRF imaging of pLAT-Alexa488 (300 molecules/μm^2) with Sos1 (0.5 μM) alone or additionally with wild-type Grb2 (0.5 μM) or Grb2ΔSH3 (1 μM) (note- concentrations were set to maintain identical total SH3 concentrations in the experiments containing Grb2 and Grb2ΔSH3). Scale bar: 2 μm. **(E)** Valency-dependent clustering of pLAT. LEFT: pLAT wild-type with three Grb2 phosphorylation sites (YYY) or mutants that contain 6 (2xYYY), 2 (FYY, YFY, YYF), 1 (FFY), or 0 (FFF) phospho-tyrosines were incubated with increasing concentrations of Grb2 and Sos1. 1x indicates 125 nM Grb2 and 62 nM Sos1. pLAT valency mutants were plated at a density around 300 molecules/μm^2. Clusters were imaged by TIRF microscopy. Scale bar: 5 μm. RIGHT: Quantification of clustering of pLAT valency mutants. Clustering degree was quantified by fractional intensity. Phase diagrams of pLAT mutants using a larger range of Grb2 and Sos1 concentrations are shown in fig. S5. Values shown are the mean ± s.d. (N=3 independent experiments).

Fig. 2. LAT clustering promotes MAPK(ERK) signaling in T cells.

(A) Fluorescence recovery after photobleaching (FRAP) of LAT-mCitrine clusters on plasma membranes of Jurkat T cells activated by anti-CD3 antibody (OKT3 at 5 μg/mL) attached to the coverslip; time 0 indicates the time of the photobleaching pulse. Scale bar, 5 μm or 1 μm on the enlarged panel. Right plot shows the time course of the recovery (mean ± s.d.) of 15 cells. **(B)** TIRF microscopy revealed cluster formation of LAT variants in activated T cells. A LAT-deficient line (Jcam2.5) stably expressing LAT variants containing 6 (2x YYY), 3 (YYY), 2 (FYY), 1 (FFY), or 0 (FFF) tyrosines for Grb2 binding, was activated by plate-presented OKT3 at 5 μg/mL. See Methods for clustering quantification. Scale Bar: 5 μm. Shown are mean ± s.e.m. (N=16-20 cells). **(C)** MAPK(ERK) activation in Jurkat T cells expressing LAT valency mutants. Cells were activated by anti-CD3 antibody OKT3 at 5 μg/mL, fixed at 10 min, and stained with an antibody to pERK (red) and a nucleus dye Hoechst (blue). Scale bar, 20 μm. Right plot shows the percentage of pERK positive cells. 200-300 cells were scored for each data point. Shown are mean ± s.e.m. (N=3 independent experiments).

Fig. 3. Reconstitution of TCR phosphorylation to LAT clustering.

(A) Schematic of components in a reaction designed to reconstitute signaling from TCR/CD3ζ phosphorylation to LAT clustering. The cytoplasmic domains of CD45, Lck, CD3ζ, and LAT were polyhistidine-tagged for membrane attachment and incubated with other components in solution. ATP was added to trigger the phosphorylation cascade. Input: CD45-SNAP-TMR, Lck, CD3ζ, and LAT-Alexa647 at 30, 250, 500, and 1000 molecules/μm^2, respectively, 10 nM ZAP70-505-Star, 250 nM Grb2, 125 nM Sos1, 250 nM Gads, 125 nM SLP-76, and 0.5 mM ATP-Mg. **(B)** TIRF microscopy revealed time courses of ZAP70 membrane recruitment, CD45 exclusion, and LAT clustering in the reconstituted pathway. A larger field view of LAT clusters

is shown in fig. S6B. Scale bar: 2 μm. **(C)** TOP: pLAT-Alexa488 (300 molecules/μm^2) bound to planar lipid bilayers was incubated with Grb2 (1 μM) in the presence (top) or absence (bottom) of Sos1 (1 μM). Then the cytoplasmic domain of CD45-TMR (4 nM; with an N-terminal His_{10} tag) was added and its localization was visualized by TIRF microscopy. Scale bar: 2 μm. BOTTOM: Quantification of fluorescence intensity of pLAT and CD45 along the line scan indicated by a white line in the top merged image. **(D)** Western blot analysis of pLAT dephosphorylation by CD45. pLAT bound to membrane (300 molecules/μm^2) was incubated with 1 μM Grb2 (unclustered pLAT) or 1 μM Grb2 plus 1 μM Sos1 (clustered pLAT). His_{10}-CD45 was then added and the reactions were stopped after 5 min by adding SDS-PAGE loading buffer containing 2 mM vanadate. Quantification of pLAT phosphorylation normalized to the total LAT signal is shown in the bottom plot.

Fig. 4. LAT clustering promotes actin polymerization.

(A) Schematic of the reconstituted signaling pathway from CD3ζ/TCR phosphorylation to actin polymerization. ZAP70-505-Star, LAT-Alexa647, and actin-Rhodamine serve as reporters for TCR phosphorylation, LAT clustering, and actin assembly, respectively. Lck, CD3ζ, and LAT were membrane attached through a polyhistidine tag and incubated with other components in solution. ATP was then added to trigger the signaling cascade. Input: same for Lck, CD3ζ, pLAT-Alexa647, and ZAP70-505-Star as described in Fig. 3A. The rest are 250 nM Gads, 125 nM SLP-76, 500 nM Nck, 250 nM N-WASp, 2.5 nM Arp2/3 complex, 500 nM actin (5% Rhodamine labeled), and 0.5 mM ATP-Mg. **(B)** Time courses of ZAP70 membrane recruitment, LAT clustering, and actin polymerization in the reconstituted assay after addition of ATP at time 0. LAT clustering was quantified as variance of fluorescence intensities on membranes (See

Methods). **(C)** TIRF imaging showing actin assembly on the LAT clusters. Scale bar: 2 μm. **(D)** TIRF imaging of pLAT-Alexa647 and actin-Rhodamine 45 min after adding ATP to the reaction. Input: same as in Fig. 4A except with higher concentrations of components of actin and actin regulators (500 nM SLP-76, 1000 nM Nck, 500 nM N-WASp, 5 nM Arp2/3 complex, 1000 nM actin (5% Rhodamine-labeled)). Scale bar: 2 μm. **(E)** LEFT: TIRF microscopy images of His_{10}-Nck-Pacific Blue and actin-Rhodamine on the bilayer. Nck (150 molecules/μm^2) was attached to the bilayer and N-WASp (5 nM), Arp2/3 complex (0.25 nM), actin (200 nM; 5% Rhodamine labeled), and 0.5 mM ATP-Mg were in solution. Increasing concentrations of His-tagged pLAT were added as indicated along with Gads and pSLP-76. At 0.1 nM pLAT, Gads, and pSLP-76 concentrations were 8 nM and 4 nM, respectively. As pLAT concentration was increased, more Gads and pSLP-76 were added to maintain a constant ratio of the clustering components. Scale bar: 2 μm. RIGHT: Mean actin fluorescence (red) and Nck clustering level (blue) quantified as variance of His_{10}-Nck fluorescence intensity, are plotted for increasing concentrations of pLAT. Shown are mean ± s.e.m. (N=3 independent experiments).

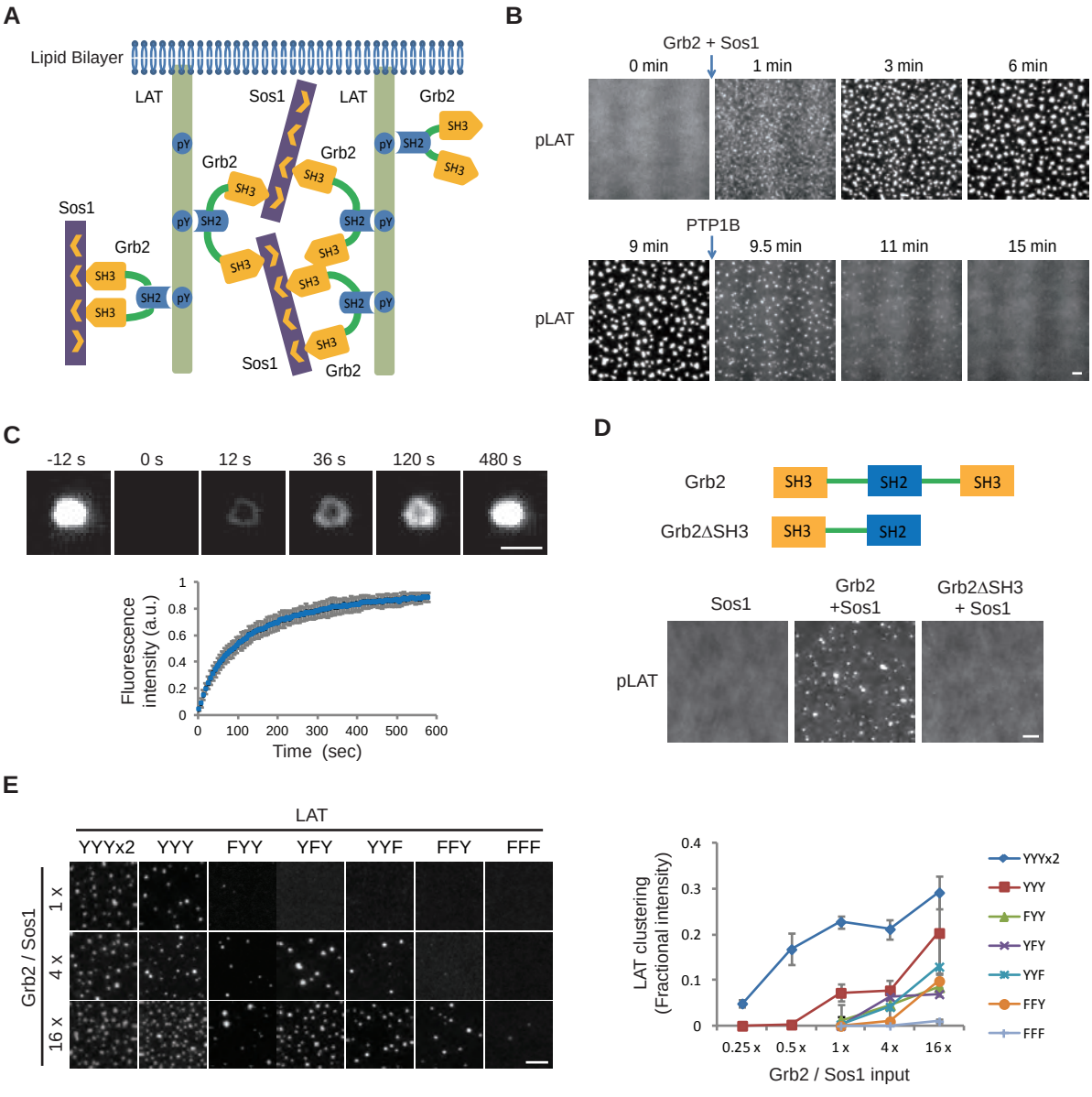
A
Lipid Bilayer
LAT
Sos1
LAT
Grb2
Grb2
Grb2
Sos1
Grb2
Sos1
Grb2
B
Grb2 + Sos1
0 min
1 min
3 min
6 min
pLAT
PTP1B
9 min
9.5 min
11 min
15 min
pLAT
C
-12 s
0 s
12 s
36 s
120 s
480 s
Fluorescence intensity (a.u.)
Time (sec)
D
Grb2
Grb2ΔSH3
Sos1
Grb2 +Sos1
Grb2ΔSH3 + Sos1
pLAT
E
LAT
YYYx2
YYY
FYY
YFY
YYF
FFY
FFF
Grb2 / Sos1
1 x
4 x
16 x
LAT clustering (Fractional intensity)
Grb2 / Sos1 input
0.25 x
0.5 x
1 x
4 x
16 x

Figure 1

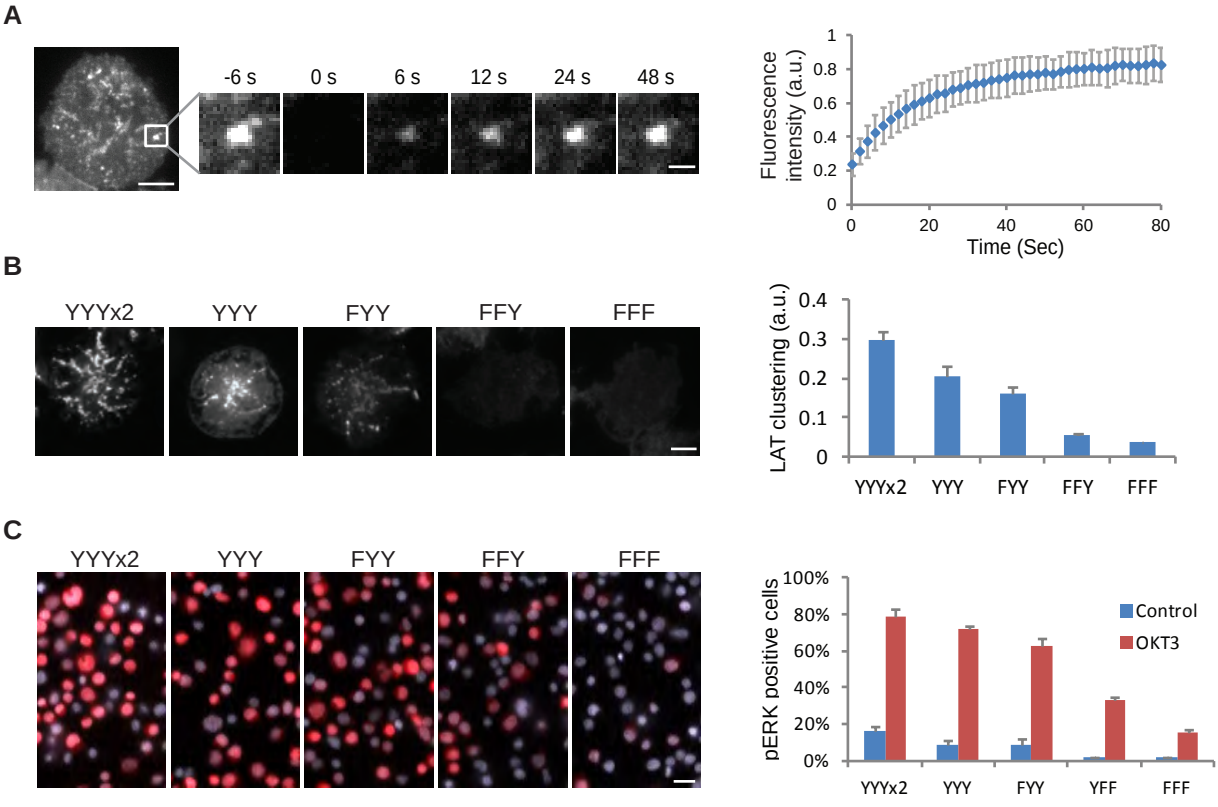
A
-6 s
0 s
6 s
12 s
24 s
48 s
Fluorescence intensity (a.u.)
Time (Sec)
B
YYYx2
YYY
FYY
FFY
FFF
LAT clustering (a.u.)
C
pERK positive cells
Control
OKT3
YFF

Figure 2

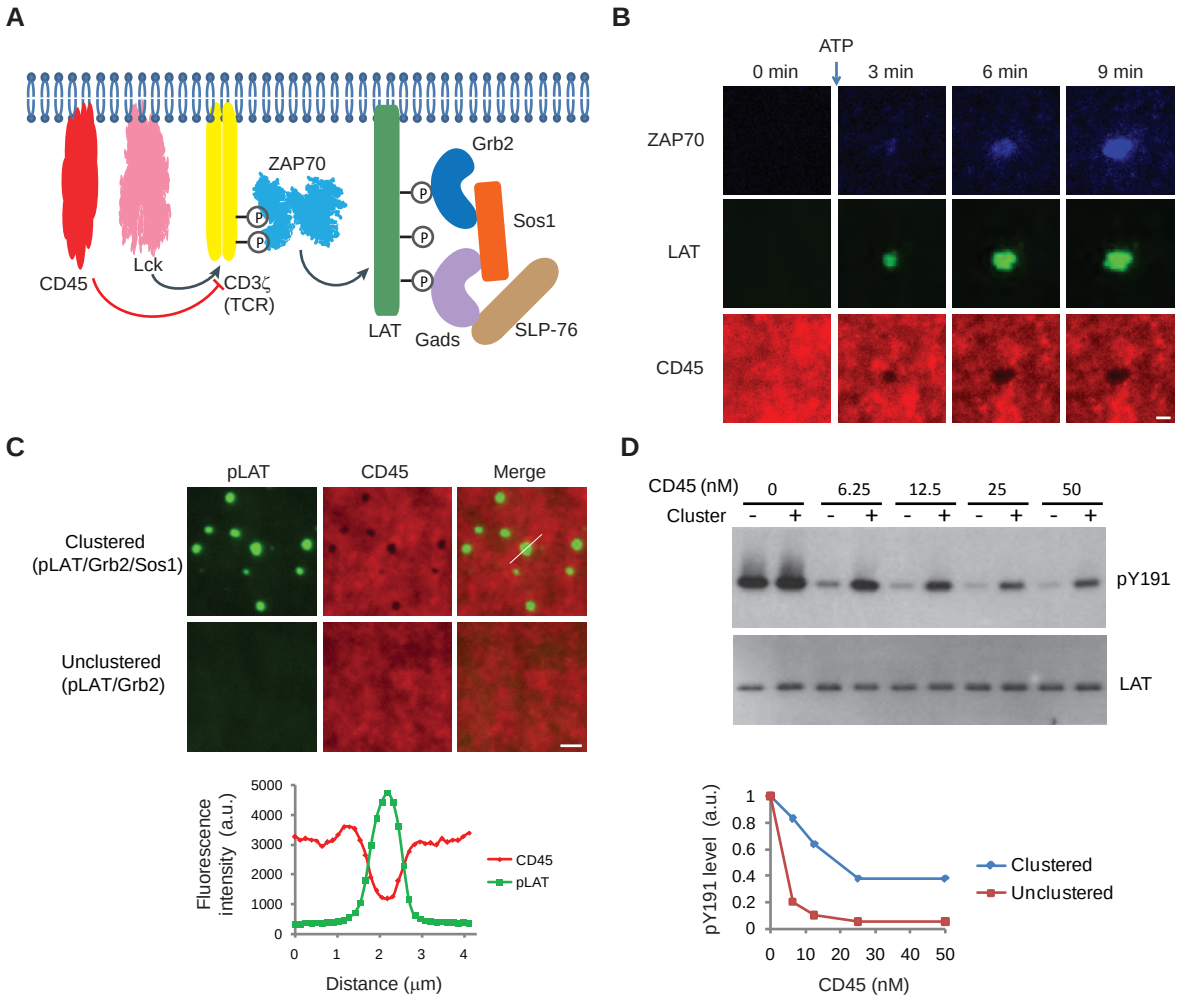
A
ZAP70
Grb2
Sos1
Lck
CD45
CD3ζ
(TCR)
LAT
Gads
SLP-76
B
ATP
0 min
3 min
6 min
9 min
ZAP70
LAT
CD45
C
pLAT
CD45
Merge
Clustered
(pLAT/Grb2/Sos1)
Unclustered
(pLAT/Grb2)
Fluorescence
intensity (a.u.)
5000
4000
3000
2000
1000
0
0
1
2
3
4
Distance (μm)
CD45
pLAT
D
CD45 (nM)
0
6.25
12.5
25
50
Cluster
- + - + - + - + - +
pY191
LAT
pY191 level (a.u.)
1
0.8
0.6
0.4
0.2
0
0
10
20
30
40
50
CD45 (nM)
Clustered
Unclustered

Figure 3

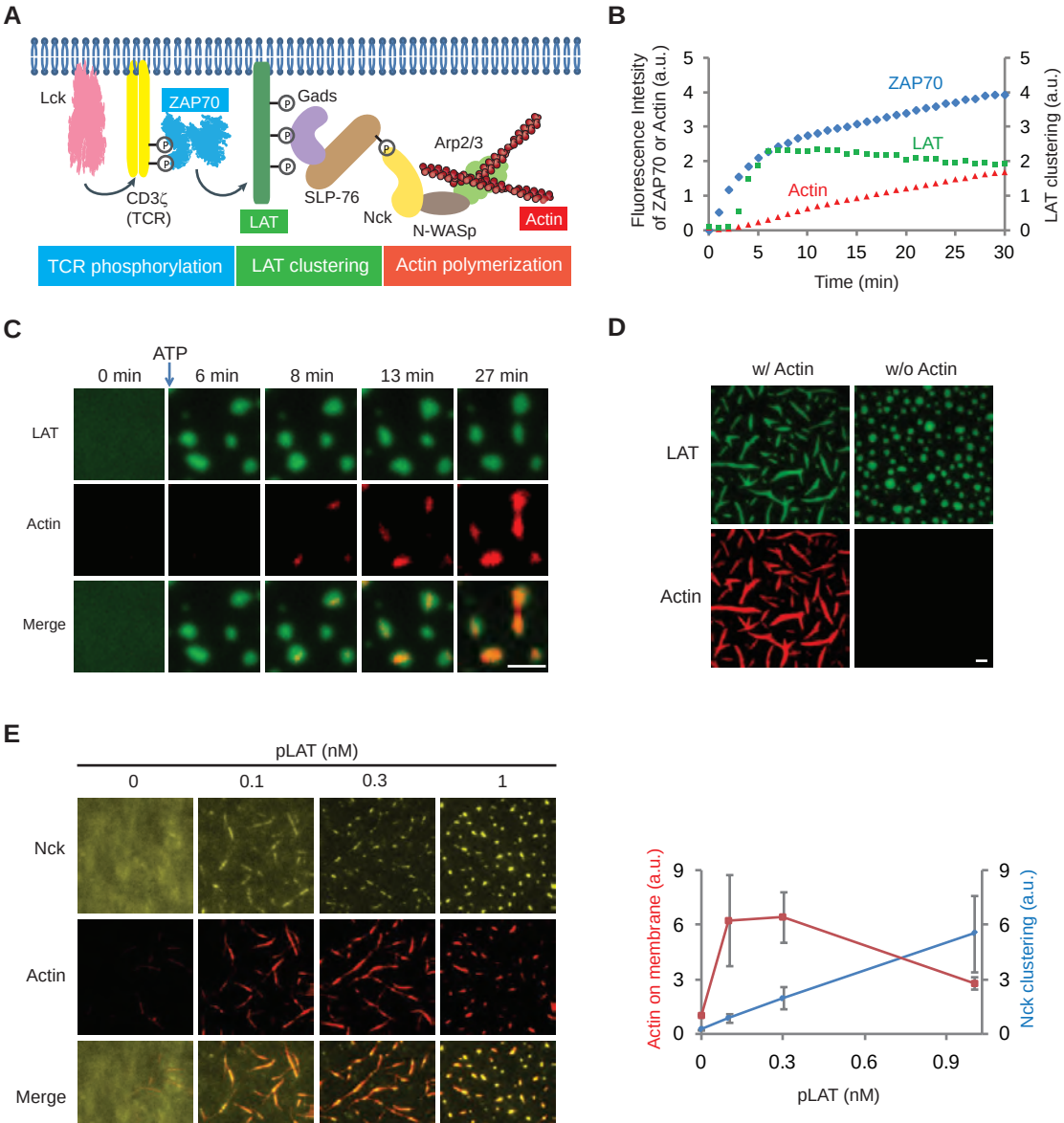
A
Lck
ZAP70
CD3ζ
(TCR)
LAT
Gads
SLP-76
Nck
Arp2/3
N-WASp
Actin
TCR phosphorylation
LAT clustering
Actin polymerization
B
Fluorescence Intetsity
of ZAP70 or Actin (a.u.)
LAT clustering (a.u.)
ZAP70
LAT
Actin
Time (min)
C
ATP
0 min
6 min
8 min
13 min
27 min
LAT
Actin
Merge
D
w/ Actin
w/o Actin
LAT
Actin
E
pLAT (nM)
0
0.1
0.3
1
Nck
Actin
Merge
Actin on membrane (a.u.)
Nck clustering (a.u.)
pLAT (nM)

Figure 4

Supplementary Materials for

Phase separation of signaling molecules promotes T cell receptor signal transduction

Xiaolei Su*, Jonathon A. Ditlev*, Enfu Hui, Wenmin Xing, Sudeep Banjade, Julia Okrut, David S. King, Jack Taunton, Michael K. Rosen‡, and Ronald D. Vale‡

correspondence to: ron.vale@ucsf.edu; michael.rosen@utsouthwestern.edu
*Equal contributions; ‡ Co-corresponding authors

This PDF file includes:

Other Supplementary Materials for this manuscript includes the following:

Movies S1 to S5

Materials and Methods

Protein reagents

Human LAT (aa 48-233) or tyrosine mutants with an N-terminal His_8 tag, CD3ζ (aa 52-164) with an N-terminal His_{10} tag or additionally a C-terminal SNAP tag, Grb2 (aa 1-217), Grb2 (aa 1-154), Sos1 (aa 1117-1319), SLP-76 (aa 101-420), Gads (aa 1-155 and 261-330) with an internal GB1 tag, Nck1 (aa 1-377) with or without an C-terminal His_{10} tag, PTP1B (aa 3-277), and Rat N-WASp (aa 151-501), SNAP or charge mutants with an N-terminal His_{10} tag, GFP or charge mutants with an N-terminal His_{10} tag, and FKBP with an N-terminal His_{10} tag and a C-terminal SNAP tag were expressed and purified from bacteria. Lck (aa 3-509) with an N-terminal His_{10} tag, ZAP70 (aa 1-619) with an N-terminal SNAP tag, CD45 (aa 598-1304) with an N-terminal His_{10} tag and a C-terminal SNAP tag were expressed and purified from Sf9 cells. Arp2/3 complex was purified from Bovine thymus. Actin (rabbit skeletal muscle) and Rhodamine-labeled actin were purchased from Cytoskeleton. Purified products are shown in fig. S1A. Details of constructs used in this study are listed in the table S1.

Protein purification

LAT purification

BL21(DE3) cells containing MBP-His_8-LAT 48-233-His_6 were collected by centrifugation and lysed by cell disruption (Emulsiflex-C5, Avestin) in 20 mM imidazole (pH 8.0), 150 mM NaCl, 5 mM βME, 0.1% NP-40, 10% glycerol, 1 mM PMSF, 1 μg/ml antipain, 1 μg/ml pepstatin, and 1 μg/ml leupeptin. Centrifugation-cleared lysate was applied to Ni-NTA agarose (Qiagen), washed with 10 mM imidazole (pH 8.0), 150 mM NaCl, 5 mM βME, 0.01% NP-40, and 10% glycerol, and eluted with the same buffer containing 500 mM imidazole (pH 8.0). The MBP tag and His_6 tag were removed using TEV protease treatment for 16 hrs at 4°C. Cleaved protein was applied to a Source 15 Q anion exchange column and eluted with a gradient of 200 mM→300 mM NaCl in 20 mM HEPES (pH 7.0) and 2 mM DTT followed by size exclusion chromatography using a Superdex 200 prepgrade column (GE Healthcare) in 25 mM HEPES (pH 7.5), 150 mM NaCl, 1 mM $MgCl_2$, and 1 mM DTT.

Grb2, Grb2ΔSH3, Gads, Sos1, and SNAP purification

BL21(DE3) cells containing GST-tagged Grb2, Grb2ΔSH3, Gads, or Sos1 were collected by centrifugation and lysed by 1 mg/mL lysozyme in PBS with 5% glycerol and 0.5 mM EDTA for 1hr at 4°C. The lysate was additionally treated with 0.5 % Triton X-100, 10 μg/mL DNase, and 1 mM $MgCl_2$ for 1 hr. Centrifuge-cleared lysate was supplemented 1 mM DTT and applied to Glutathione Sepharose 4B (GE Healthcare) and washed with 50 mM HEPES (pH 7.0), 150 mM NaCl, 5% glycerol and 1 mM TCEP. GST was cleaved from protein by PreScission protease treatment overnight at 4°C. Cleaved protein was further purified by size exclusion chromatography using a Superdex 200 prepgrade

column (GE Healthcare) in 50 mM HEPES (pH 7.5), 150 mM NaCl, 10% glycerol, and 1 mM TCEP.

Cleavable Grb2 purification

BL21(DE3) cells containing GST-Cleavable Grb2 were collected by centrifugation and lysed by sonication in 25 mM Tris-HCl (pH 8.0), 200 mM NaCl, 2 mM EDTA (pH 8.0), 5 mM βME, 1 mM PMSF, 1 μg/ml antipain, 1 μg/ml pepstatin, and 1 μg/ml leupeptin. Centrifuge-cleared lysate was applied to Glutathione Sepharose 4B (GE Healthcare) and washed with 25 mM Tris-HCl (pH 8.0), 200 mM NaCl, and 1 mM DTT. GST was cleaved from protein by TEV protease treatment for 16 hrs at 4°C. Cleaved protein was applied to a Source 15Q anion exchange column and eluted with a gradient of 150 mM→250 mM NaCl in 20 mM imidazole (pH 7.0) and 1 mM DTT followed by size exclusion chromatography using a Superdex 200 prepgrade column (GE Healthcare) in 25 mM HEPES (pH 7.5), 150 mM NaCl, 1 mM $MgCl_2$, and 1 mM βME.

SLP-76 purification and phosphorylation

BL21(DE3) cells containing MBP-SLP-76 Acidic and Proline Rich region-His_6 were collected by centrifugation and lysed by cell disruption (Emulsiflex-C5, Avestin) in 20 mM imidazole (pH 8.0), 150 mM NaCl, 5 mM βME, 0.01% NP-40, 10% glycerol, 1 mM PMSF, 1 μg/ml antipain, 1 μg/ml pepstatin, and 1 μg/ml leupeptin. Centrifuge-cleared lysate was applied to Ni-NTA Agarose (Qiagen), washed first with 20 mM imidazole (pH 8.0), 150 mM NaCl, 5 mM βME, 0.01% NP-40, 10% glycerol, and 1 mM benzamidine, then washed with 50 mM imidazole (pH 8.0), 300 mM NaCl, 5 mM βME, 0.01% NP-40, 10% glycerol, 1 mM benzamidine, and eluted with 500 mM imidazole (pH 8.0), 150 mM NaCl, 5 mM βME, 0.01% NP-40, 10% glycerol, and 1 mM benzamidine. MBP cleaved by TEV protease treatment for 16 hrs at 4°C or for 2 hrs at room temperature. His_6 was concurrently cleaved by PreScission protease treatment for 16 hrs at 4°C or for 2 hrs at room temperature. Cleaved protein was applied to a Source 15Q anion exchange column and eluted with a gradient of 200 mM→350 mM NaCl in 20 mM HEPES (pH 7.5) and 2 mM βME followed by size exclusion chromatography using a Superdex 200 prepgrade column (GE Healthcare) in 25 mM HEPES (pH 7.5), 150 mM NaCl, 1 mM $MgCl_2$, and 1 mM DTT. To phosphorylate SLP-76, Purified SLP-76 was incubated in 50 mM HEPES (pH 7.0), 150 mM NaCl, 20 mM $MgCl_2$, 15 mM ATP, 2 mM DTT, and 20 nM Active GST-ZAP70 (SignalChem). Phosphorylated SLP-76 was resolved on a MonoQ anion exchange column (GE Healthcare) using a shallow %B gradient from 300 mM→400 mM over 60 column volumes to separate differentially phosphorylated species of SLP-76. 3pY SLP-76 was confirmed by mass spectrometry analysis.

Nck purification

BL21(DE3) cells containing GST-Nck1 were collected by centrifugation and lysed by sonication in 25 mM Tris-HCl (pH 8.0), 200 mM NaCl, 2 mM EDTA (pH 8.0), 1 mM DTT, 1 mM PMSF, 1 μg/ml antipain, 1 μg/ml pepstatin, and 1 μg/ml leupeptin. Centrifuge-cleared lysate was applied to Glutathione Sepharose 4B (GE Healthcare) and washed with 25 mM Tris-HCl (pH 8.0), 200 mM NaCl, and 1 mM DTT. GST was

cleaved from protein by TEV protease treatment for 16 hrs at 4°C. Cleaved protein was applied to a Source 15Q anion exchange column and eluted with a gradient of 0 → 200 mM NaCl in 20 mM imidazole (pH 7.0) and 1 mM DTT. Eluted protein was pooled and applied to a Source 15S cation exchange column and eluted with a gradient of 0 → 200 mM NaCl in 20 mM imidazole (pH 7.0) and 1 mM DTT. Eluted protein was concentrated using Amicon Ultra 10k concentrators and further purified by size exclusion chromatography using a Superdex 75 prepgrade column (GE Healthcare) in 25 mM HEPES (pH 7.5), 150 mM NaCl, and 2 mM βME.

N-WASp and His-Nck purification

BL21(DE3) CodonPlus RILcells expressing His_6-N-WASp 151-501 or His_{10}-Nck1 were collected by centrifugation and lysed using amicrofluidizer in 20 mM HEPES (pH 7.5), 500 mM NaCl, 10 mM imidazole, 30 mM L-Arg, 10% glycerol, 4 mM benzamidine, and 2 mM βME. Centrifuge-cleared lysate was applied to Ni-NTA Agarose (Qiagen), washed first with 20 mM HEPES (pH 7.5), 1000 mM NaCl, 30 mM L-Arg, 10% glycerol, 2 mM βME, then washed with 20 mM HEPES (pH 7.5), 500 mM NaCl, 10 mM imidazole, 30 mM L-Arg, 10% glycerol, 4 mM benzamidine, 2 mM βME, 50 mM KCl, 10 mM $MgCl_2$, and 2 mM ATP, followed by elution with 20 mM HEPES (pH 7.5), 500 mM NaCl, 400 mM imidazole, 30 mM L-Arg, and 10% glycerol, 1 mM TCEP. The His_6 tag on N-WASp was cleaved with TEV protease overnight on ice. TEV-cleaved N-WASp was applied to a Heparin column in 20 mM HEPES (pH 7.5), 0.5 mM TCEP and purified using a 50 → 1500 mM NaCl gradient. His_{10}-Nck1 was further purified by size exclusion chromatography using a Superdex 200 prepgrade column (GE Healthcare) in 20 mM HEPES (pH 7.5), 500 mM NaCl, 10% glycerol, and 0.5 mM TCEP.

PTP1B purification

BL21(DE3) cells containing GST-PTP1B were collected by centrifugation and lysed by sonication in 20 mM Tris-HCl (pH 8.0), 200 mM NaCl, 2 mM EDTA (pH 8.0), and 1 mM DTT. Centrifuge-cleared lysate was applied to Glutathione Sepharose 4B (GE Healthcare), washed with 25 mM Tris-HCl (pH 8.0), 200 mM NaCl, and 1 mM DTT. GST was cleaved by PreScission protease treatment for 16 hrs at 4°C. Cleaved protein was applied to a Source 15Q anion exchange column and eluted with a gradient of 0 → 300 mM NaCl in 20 mM imidazole (pH 7.0) and 1 mM DTT followed by size exclusion chromatography using a Superdex 200 prepgrade column (GE Healthcare) in 25 mM HEPES (pH 7.5), 150 mM NaCl, and 1 mM βME.

FKBP-SNAP, CD3ζ and Lck purification

The cytosolic domain of human CD3ζ (residues 52-164) was expressed with an N-terminal His_{10} tag in BL21(DE3) *E. coli*. Full length human Lck (with a G2A mutation to prevent myristoylation) with an N-terminal His_{10}-tag was expressed in SF9 cells using the Bac-to-Bac baculovirus expression system (Life Technologies). The proteins were purified using Ni-NTA Agarose (Qiagen) and size exclusion chromatography essentially as described previously *(22)*.

CD45 purification

The cytosolic portion of human CD45 (residues 598-1304) with an N-terminal His_{10} tag and a C-terminal SNAP tag was expressed in SF9 cells using the Bac-to-Bac baculovirus expression system (Life Technologies). Cells were harvested by centrifugation and lysed by Dounce homogenizer in 50 mM HEPES (pH 7.4), 300 mM NaCl, 30 mM imidazole, 5% glycerol, 5 μg/mL DNase, 0.5% Triton X-100, 0.5 mM TCEP, 1 mM PMSF, and protease inhibitor cocktail. Centrifuge-cleared lysate was applied to Ni sepharose (GE healthcare), washed with 50 mM HEPES (pH 7.4), 300 mM NaCl, 5% glycerol, 15 mM imidazole, and 1 mM TCEP, and eluted with the same buffer with additional 400 mM imidazole. Eluted protein was further purified by size exclusion chromatography using a Superdex 200 prepgrade column (GE Healthcare) in 50 mM HEPES (pH 7.5), 150 mM NaCl, 10% glycerol, and 1 mM TCEP.

ZAP70 purification

Human ZAP70 with an N-terminal SNAP tag was expressed as a GST fusion protein in SF9 cells using the Bac-to-Bac baculovirus expression system (Life Technologies), with a PreScission recognition sequence (LEVLFQGP) engineered between the GST and SNAP tag. The baculovirus infected cells were lysed in an Emulsiflex system (Avestin) in 50 mM HEPES (pH 7.5), 150 mM NaCl, supplemented with 5 mM βME,1 mM PMSF, 1 mM benzamidine, and complete protease inhibitor (Roche), then subjected to centrifugation at 30,000 x g for 20 min. The cleared lysate was incubated with Glutathione Sepharose 4B (GE Healthcare) for 3 hr at 4 °C before washed with 3 x 50 mL HEPES buffered saline. In order to remove the GST moiety, the bead slurry was treated with PreScission protease. The supernatant fraction containing soluble proteins was then subjected to size exclusion chromatography, and the monomeric fractions were collected.

Phosphorylation and isolation of 4pY LAT

Purified plain LAT was concentrated using Amicon Ultra Centrifugal Filter units (Millipore) to >400 μM, mixed with 25 mM HEPES (pH 7.5), 150 mM NaCl, 15 mM ATP, 20 mM $MgCl_2$, 2 mM DTT and active GST-ZAP70 (SignalChem), and incubated for 24 hrs at 30°C. Phosphorylated LAT was resolved on a MonoQ anion exchange column using a shallow NaCl gradient to separate differentially phosphorylated species of LAT (fig. S1B). 4pY LAT was confirmed by mass spectrometry.

Maleimide-conjugated dye labeling of proteins

Cysteine-containing LAT, pLAT, Grb2, Nck, SLP-76 and Sos1 were exchanged into buffer containing no reducing agent (25 mM HEPES (pH 7.0), 150 mM NaCl, 1 mM EDTA) using a HiTrap Desalting Column. C_5-maleimide Alexa488, TMR, Pacific Blue, or C_2-maleimide Alexa647 were added in excess and incubated with protein for 16 hrs at 4°C or 2 hrs at room temperature. Following the incubation, 5 mM 2-mercaptoethanol was added to the mixture to quench the labeling reaction. Excess dye was removed from labeled protein by size exclusion chromatography.

Protein concentrations for in vitro reconstitution

Overall, we sought to use physiologically relevant concentrations of proteins in the in vitro reconstitution reactions. The membrane density of LAT in T cells was estimated to be 100-1200 molecules/μm^2 *(19,28)*. We used 300 molecules/μm^2 in most of the assays and 1000 molecules/μm^2 in some assays. To determine the membrane density of pLAT on SLBs, 1 pM of pLAT-Cy3B was mixed with nanomolar concentrations of pLAT-Alexa488 and attached to membranes. The numbers of pLAT-Cy3B molecules in a given area were counted by single molecule imaging and used, along with the [pLAT-Cy3B]/[pLAT-Alexa488] ratio to calculate overall density of pLAT on SLBs. On average, 3 nM of added pLAT or other membrane-bound proteins gives a density around 300 molecules/μm^2 in our experimental settings. The membrane densities of TCR, Lck, and CD45 were estimated to be 110-360 molecules/μm^2, 140-430 molecules/μm^2, and 360-1800 molecules/μm^2, respectively *(22)*. The total concentrations of Grb2, Sos1, Gads were estimated as 1.5-6.9 μM, 0.4-0.7 μM, and 1.5-5.7 μM, respectively *(19,28)*. The protein concentrations used in this study are mostly within these ranges.

Small Unilamellar Vesicle Preparation

Synthetic 1,2-dioleyl-*sn*-glycero-3-phosphocholine (POPC), 1,2-dioleoyl-*sn*-glycero-3-[(*N*-(5-amino-1-carboxypentyl)iminodiacetic acid)succinyl] (nickel salt, DGS-NTA-Ni) and 1,2-dioleoyl-*sn*-glycero-3-phosphoethanolamine-N-[methoxy(polyethyleneglycol)-5000] (ammonium salt) (PEG5000 PE) were purchased from Avanti Polar Lipids. Phospholipids (98% POPC, 2% DGS-NTA-Ni and 0.1% PEG 5000 PE) were dried under a stream of Argon, desiccated over 3 hrs and resuspended in PBS. To promote the formation of small unilamellar vesicles (SUVs), the lipid solution was repeatedly frozen in liquid N_2 and thawed using a 37°C water bath until the solution cleared. Cleared SUV-containing solution was centrifuged at 33,500g for 45 min at 4°C. Supernatant containing SUVs was collected and stored at 4°C covered with Argon.

Reconstitution assay on supported lipid bilayers

Supported lipid bilayers (SLBs) were formed in 96-well glass-bottomed plates (Matrical). Glass was washed with Hellmanex III (Hëlma Analytics) overnight, thoroughly rinsed with MilliQ H_2O, washed with 5M NaOH for 1 hr at 50°C for three times, and thoroughly rinsed with MilliQ H_2O followed by equilibration with 50 mM HEPES (pH 7.5), 150 mM NaCl, and 1 mM TCEP. SUVs were added to cleaned wells covered by 50 mM HEPES (pH 7.5), 150 mM NaCl, and 1 mM TCEP. Wells were incubated for 1 hr at 42°C to allow SUVs to collapse on glass and fuse to form SLB. SLBs were washed with 50 mM HEPES (pH 7.5), 150 mM NaCl, and 1 mM TCEP to remove excess SUVs. SLBs were blocked with clustering buffer (50 mM HEPES (pH 7.5), 150 mM NaCl, 1 mM TCEP, and 1 mg/mL BSA) for 30 min at room temperature. Indicated concentrations of His-tagged proteins were premixed and incubated with SLBs for about 3 hrs. SLBs were washed with clustering buffer to remove unbound His-tagged proteins. Indicated amounts of soluble proteins were added to His-tagged protein-bound SLBs and imaged using TIRF microscopy. Microscopy experiments were performed in the presence of a glucose/glucose oxidase/catalase O_2-scavenging system. For signaling reconstitution

assays, the final reaction buffer is 35 mM HEPES (pH 7.2), 60 mM NaCl, 30 mM KCl, 1 mM $MgCl_2$, 0.4 mM TCEP, and 0.4 mg/mL BSA.

Western blot

Reaction mixture of the dephosphorylation assay was applied to SDS-PAGE, transferred onto a nitrocellulose membrane, and incubated with a phospho-specific antibody that recognizes LAT pY191 (CST #3584, at 1:500 dilution) or a LAT plain antibody (EMD Millipore #05-770,1:500 dilution).

Cell culture and transfection

The Jurkat T cells were grown in RPMI-1640 supplemented with 10% FBS, 2 mM L-glutamine, 100 U/mL penicillin, and 100 μg/mL Streptomycin. Lentiviral transduction was used to make cells stably expressing LAT variants. LAT variants were inserted into the pHR-mCitrine-tWPRE backbone vector and introduced into a LAT-deficient Jurkat line (JCam2.5). Cells expressing similar levels of LAT variants were selected by FACS.

Activation of Jurkat T cells

Jurkat T cells were rested in RPMI-1640 media supplemented with 20 mM HEPES (pH 7.4) for 30 min before being dropped onto coverslips coated with anti-CD3ε antibody OKT3 (eBioscience #16-0037-85, 1:200 dilution). After 10 min, cells were fixed by 3.2% paraformaldehyde, permeabilized with methanol, and sequentially stained with an anti-pERK antibody (CST #9101, 1:500 dilution), a goat anti-rabbit IgG-Alexa647 (Invitrogen #A21244, 1:1000), and a nucleic acid dye Hoechst (1:10,000). The samples were imaged by fluorescence microscopy. For imaging LAT cluster formation, Jurkat T cells resuspended in RPMI-1640 media without phenol red supplemented with 20 mM HEPES (pH7.4) were dropped onto OKT3 (5 μg/mL)-coated coverslip. TIRF microscopy was used to monitor cluster formation. It was critical to set a low-angle TIRF so that only the LAT fluorescent signal on plasma membranes, but not from endocytic vesicles, was captured. For imaging LAT cluster mobility, mobilized OKT3 was presented to T cells. In brief, a supported lipid bilayer containing 1% PEG2000-Biotin and 1% DOGS-NTA was incubated with 1 μg/mL streptavidin, 1 μg/mL His-ICAM-1, and then 5 μg/mL Biotin-OKT3. Wild-type Jurkat T cells (E6.1) expressing LAT-mCherry were dropped onto the bilayers. Cluster mobility was imaged by TIRF microscopy.

Microscopy

TIRF images were captured using a Nikon Eclipse Ti microscope base equipped with an AndoriXon Ultra 897 EM-CCD camera with a 100 X 1.49 NA objective, a TIRF/iLAS2 TIRF/FRAP module (Biovision) mounted on a Leica DMI6000 microscope base equipped with a Hamamatsu ImagEMX2 EM-CCD camera with a 100 X 1.49 NA objective, or a Nikon Eclipse Ti microscope base equipped with a Hamamatsu ORCA Flash 4.0 camera with a 100 X 1.49 NA objective. Spinning disk images were capture using a Nikon Eclispe Ti microscope base equipped with an Andor EM-CCD CSU-X1

camera with a 100 X 1.49 N/A objective. FRAP was performed using a Nikon Eclipse Ti microscope base equipped with Rapp UGA-40 Phototargeter.

Data analysis and display

Images were analyzed using ImageJ (FIJI). The same brightness and contrast were applied to images within the same panels. Camera background was subtracted before calculating mean fluorescence intensities. Variance, as a means for quantifying clustering level *(18)*, was calculated as square of standard deviation of pixel intensities of the entire image. The fractional intensity calculations were used to determine phase separation. The triangle thresholding algorithm in FIJI was used to threshold images. Anything with a fractional intensity of greater than 2X the control was determined to be phase separated. Data from image analysis within FIJI was graphed using Microsoft Excel.

Supplementary Text

LAT cluster size

Previous reports suggested that LAT and TCR form nanometer-sized clusters prior to TCR activation *(29-31)*. The presence of these nanoclusters (though not a part of our in vitro reconstitution) could nucleate the formation of larger microclusters upon T cell activation in living cells and accelerate the rate of clustering and downstream signaling.

The size of LAT microclusters in vivo tend to be smaller (e.g. diffraction limit to 0.5 μm *(7,30)*) than those that form in vitro at the physiological reported concentrations of LAT/Grb2/Sos1 concentrations measured in T cells *(19, 28)* (although note that size decreases at lower concentrations of these components in vitro (fig. S1C)). Several reasons (not mutually exclusive) could account for this difference. First, a subset of these molecules (e.g. Grb2) might be bound to other components in cells, thereby reducing their effective concentrations and cluster size as we have seen also in vitro. Second, more proteins in cells might bind to LAT clusters than are included in our simplified protein reactions and affect cluster size. Third, the acto-myosin network at the plasma membrane may actively regulate microcluster size by creating filament boundaries that prevent microcluster fusion into larger clusters. Fourth, additional mechanisms in T cells could regulate microcluster size, such as lipid microdomains on the plasma membrane.

In vitro, the size of LAT clusters formed in a minimal condition with Grb2 and Sos1 is smaller than that in the complete reconstituted signaling pathway (table S2), suggesting that the cluster size is affected by the composition and concentration of components.

Regarding the time dependence of pLAT clusters in vitro, one might expect that pLAT puncta should eventually coalesce into a single domain, due to a combination of fusion and Ostwald ripening (the flux of molecules from small puncta to large puncta in order to minimize line tension in the system). However, in practice this does not occur, even after ~12 hours of incubation. This is likely due in part to the fact that as LAT clusters grow larger, their mobility decreases, and thus they stop fusing with one another. This lack of

mobility may be due to small defects on the planar bilayers that form during long reactions and anchor pLAT molecules to the glass. These defects may also decrease molecular diffusion, which will also slow Ostwald ripening.

Mechanisms of protein exclusion from the LAT clusters

We showed that CD45 was excluded from LAT clusters in vitro (Fig. 3B,C). The exclusion was observed using other membrane-bound proteins and the exclusion level correlated with the estimated isoelectric point of the proteins (fig. S7A). To test whether charge is a key parameter governing partitioning, we added negatively- or positively-charged residues to membrane-bound SNAP protein and found that addition of negative charge favored exclusion from LAT clusters while positive charge resulted in enrichment (fig. S7B). The same trend was confirmed using membrane-bound GFP variants with different charges (fig. S7C). LAT is highly charged (pI 4.6, charge -25 at physiological conditions). Based on the data above, we propose that charge affects the partitioning of membrane-bound molecules to LAT clusters.

The extracellular domain of CD45 was shown to mediate CD45 exclusion from the TCR microclusters in a size-dependent manner *(32)*. Here we show that the intracellular domain of CD45 could also mediate exclusion from LAT clusters, likely in a charge-dependent manner. This could facilitate the exclusion exerted by the extracellular domain to further enhance the stability of T cell microclusters and phosphorylation of molecules inside the clusters.

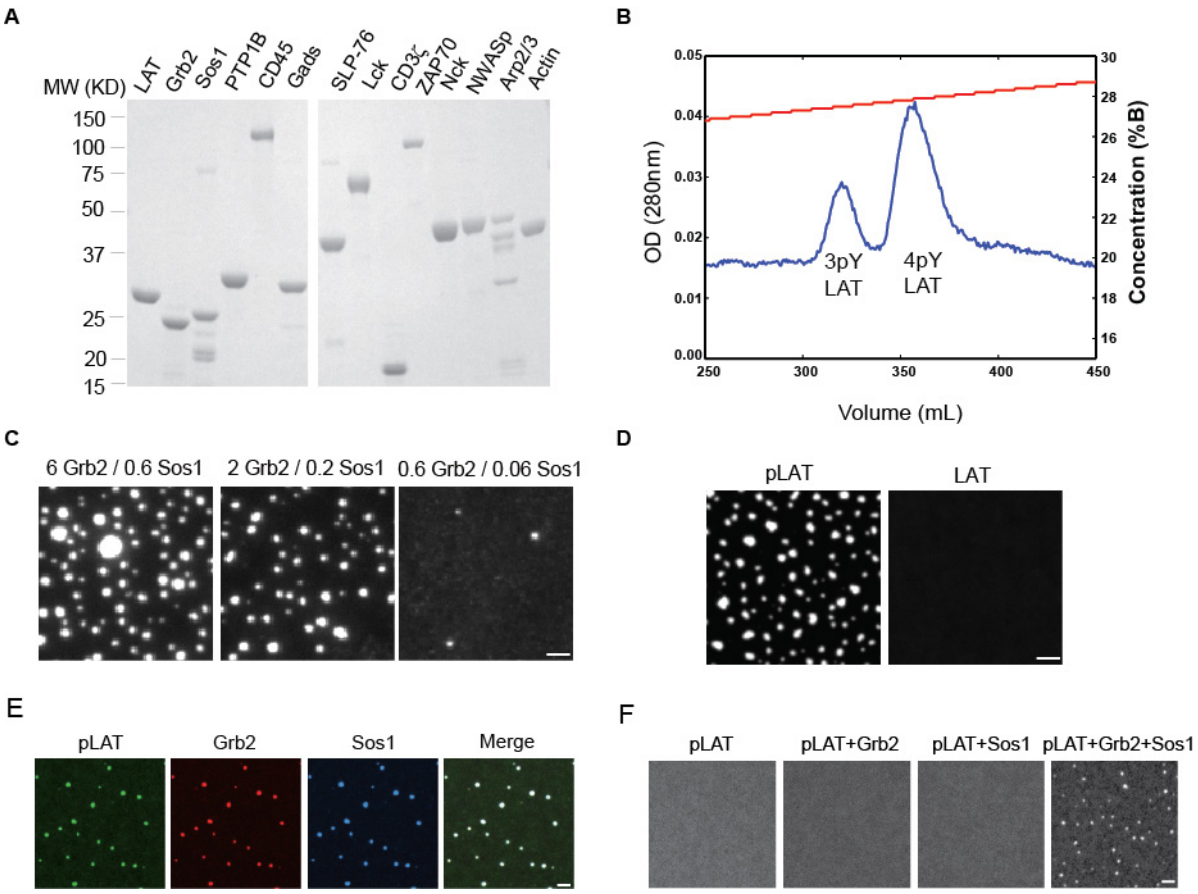

Fig. S1. pLAT forms clusters with Grb2 and Sos1 on supported lipid bilayers. (A) Purified proteins used in this study were displayed by SDS-PAGE (stained with Coomassie blue). **(B)** Separation of LAT phosphorylation products by ion exchange chromatography. Red line shows increase in percentage of B buffer. Blue line shows protein peaks detected at A_{280} following elution from the Mono Q anion exchange column. The 4pY peak was confirmed by mass spectrometry. **(C)** pLAT formed clusters with Grb2 and Sos1 at the indicated concentrations (unit μM). Scale bar: 2 μm. **(D)** Unphosphorylated LAT did not form clusters with Grb2 and Sos1. Scale bar: 2 μm. **(E)** Colocalization of pLAT-Alexa488, Grb2-Alexa568, and Sos1-Alexa647 in the cluster. Scale bar: 2 μm. **(F)** Grb2 and Sos1 are both required to form LAT clusters. pLAT-Alexa488 was incubated with either Grb2 or Sos1 or both and visualized by TIRF microscopy. Scale bar: 2 μm.

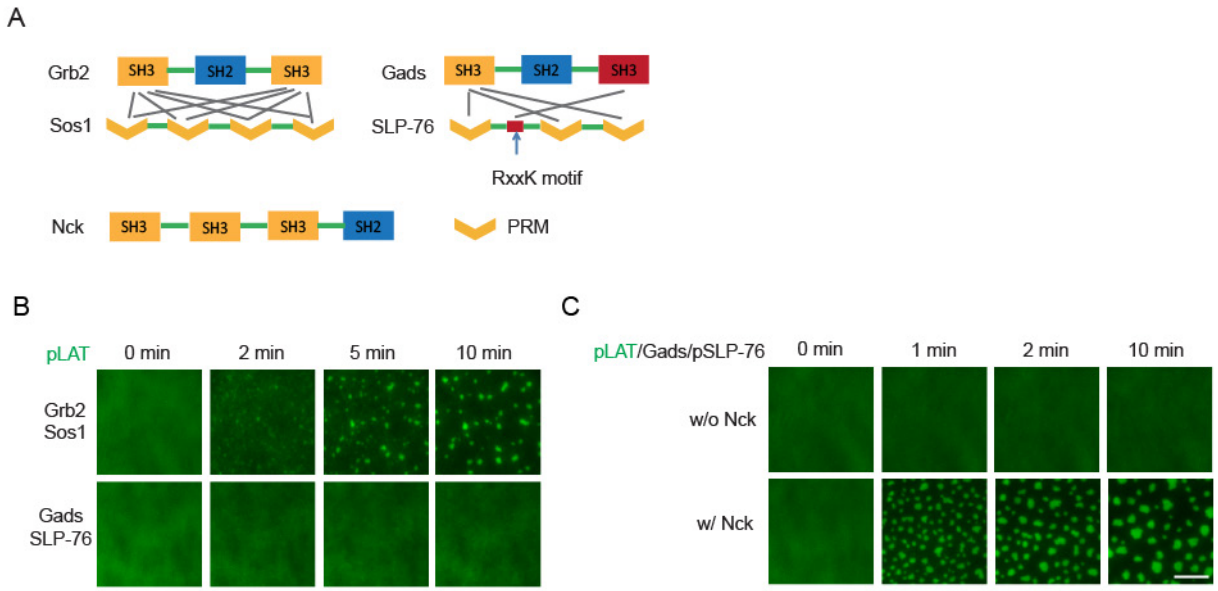

Fig. S2 Comparison of Grb2/Sos1 and Gads/SLP-76 in promoting LAT cluster formation. (A) Domain schematic and interactions of different SH2-SH3 adaptors. **(B)** TIRF imaging revealed kinetics of pLAT clustering with Grb2/Sos1 or Gads/SLP-76. pLAT-Alexa-488 (300 molecules/μm^2) was incubated with 0.5 μM Grb2 and 0.25 μM Sos1, or 0.5 μM Gads and 0.25 μM SLP-76 at time 0. Scale bar: 5 μm. **(C)** TIRF microscopy revealed that Nck promotes pLAT/Gads/pSLP76 clustering. Gads and pSLP-76, with or without 0.5 μM Nck were added at time 0. Scale bar: 5 μm.

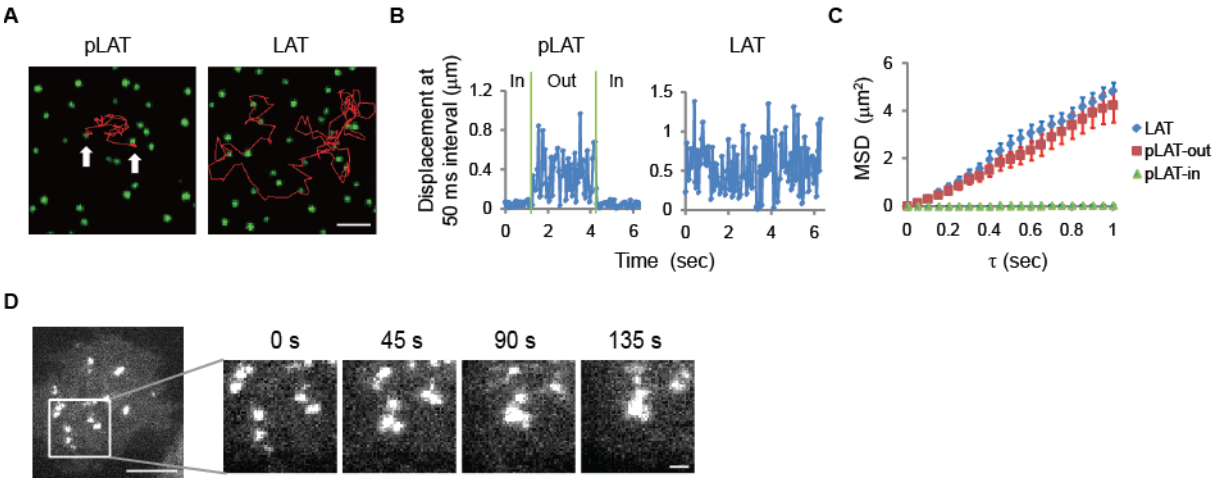

Fig. S3. Dynamics of LAT clusters. (A) Single molecule trajectories of pLAT or LAT (labeled with TMR) in the context of pLAT clusters (labeled with Alexa488). White arrows indicate trapping of a single pLAT-TMR molecule in a cluster. pLAT-Alexa488 (300 molecules/μm^2) was incubated with Grb2 (0.5 μM) and Sos1 (0.25 μM). pLAT-TMR or LAT-TMR was included at 0.07 molecules/μm^2. Scale bar, 2 μm. **(B)** Quantification of mobility of pLAT and LAT molecules shown in the left panel. The periods of time in which pLAT colocalized within the cluster ("in") or was present outside the cluster ("out") are indicated. **(C)** Mean square displacement analysis of single molecules of LAT, pLAT in cluster, and pLAT out of cluster. Shown are mean ± s.e.m. (N=15 tracks). **(D)** Fusion of LAT clusters on the plasma membrane of Jurkat T cells. Jurkat T cells expressing LAT-mCherry were plated on supported lipid bilayer functionalized with anti-CD3 antibody OKT3 and adhesive molecule ICAM-1. Mobility of microclusters was visualized by TIRF microscopy. Scale bar, 5 μm or 1 μm on the enlarged panel.

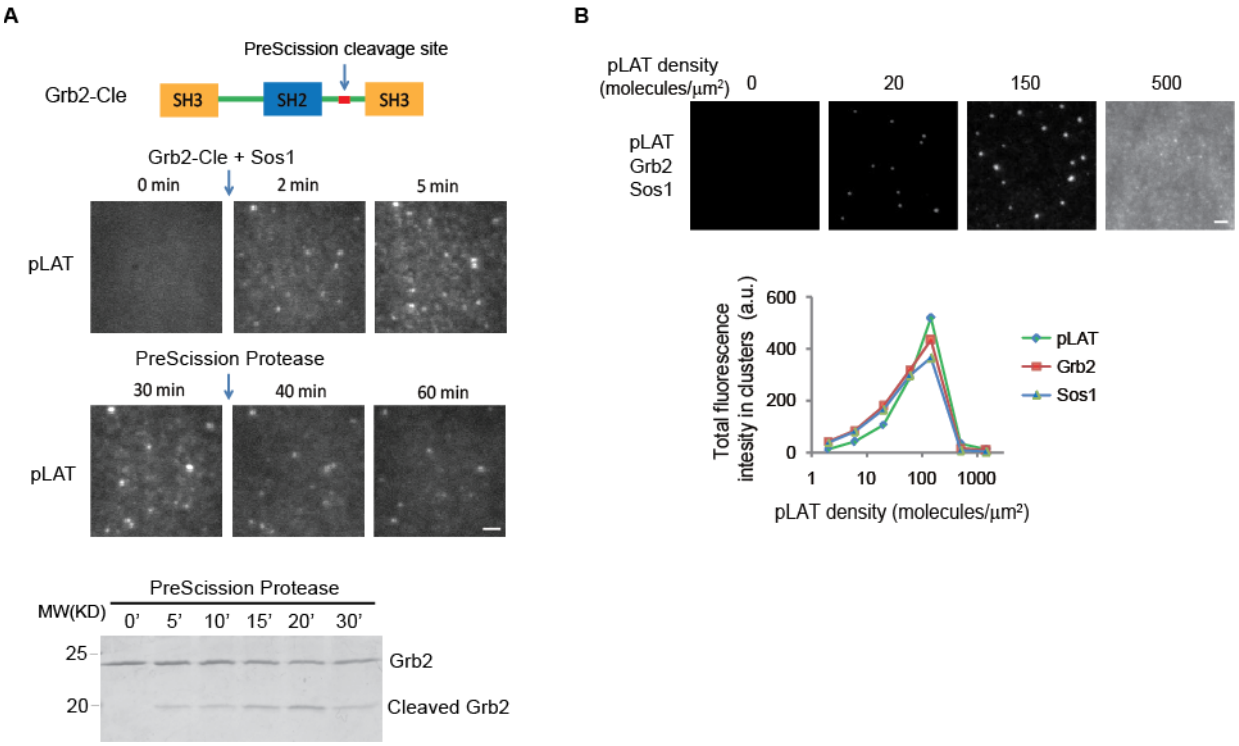

Fig. S4. Multivalent interaction-mediated LAT cluster formation. (A) TOP: Schematics of Grb2-Cle that contains a PreScission cleavage site between the SH2 and C-terminal SH3 domain. MIDDLE: TIRF imaging of pLAT-Alexa488 (300 molecules/um^2) incubated with Grb2-Cle (0.5 μM) and Sos1 (0.25 μM). Clusters were disassembled when treated with PreScission protease (50 nM). Scale bar: 2 μm. BOTTOM: Cleavage of Grb2-Cle over the course of 30 min by PreScission protease. Grb2 (0.5 μM), Sos1 (0.25 μM), and PreScission (50 nM) were mixed and incubated for 0, 5, 10, 15, 20, or 30 min at room temperature. Samples were applied to SDS-PAGE and stained by Coomassie blue. **(B)** An increasing density of pLAT-Alexa488 on the membrane was incubated with Grb2-Alexa568 (125 nM) and Sos1-Alexa647 (62 nM). Images show pLAT-Alexa488 clustering. Scale bar: 2 μm. Plot shows total fluorescence intensities of pLAT, Grb2, or Sos1 in clusters as a function of pLAT densities. A multivalent interaction model predicts this biphasic concentration dependence of LAT clustering *(19)*. Briefly, phase separation occurs due to the large size of oligomers formed by multivalent interactions. At low to intermediate concentrations, each pLAT can bind multiple Grb2 molecules, which will facilitate multivalent crosslinking (see schematic in Fig. 1A). However, at high concentrations, each pLAT can at most bind one Grb2, which will attenuate crosslinking and lead to a decrease in clustering level.

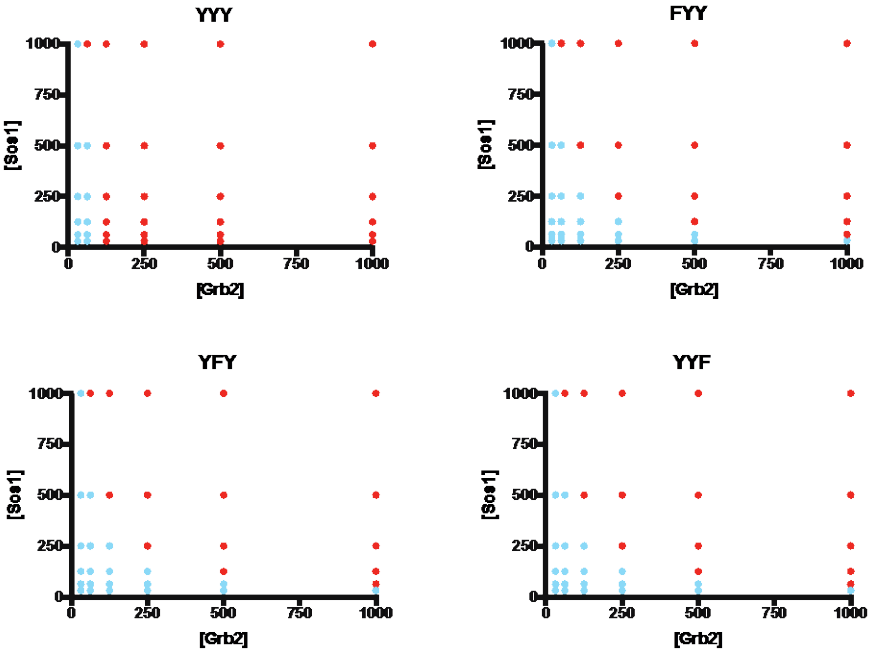

Fig. S5. Phase diagrams of pLAT and single LAT Y to F mutants. pLAT and pLAT Y to F mutants were attached to the bilayer at ~300 molecules / μm^2. Increased concentrations (unit nM) of Grb2 and Sos1 resulted in phase separation. The critical concentration of pLAT YYY (upper left) with Grb2 and Sos1 was lower than the critical concentration of each mutant (upper right, lower left, lower right). Blue dots indicate no phase separation, red dots indicate phase separation. See Methods for quantification.

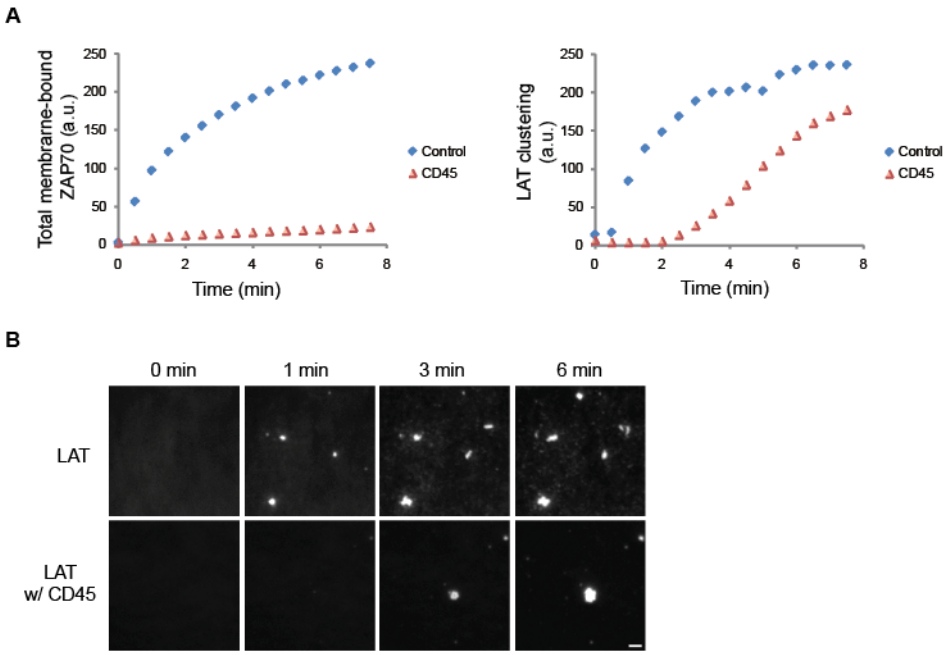

Fig. S6. TCR/CD3ζ-induced LAT clustering. (A) Time courses of ZAP70 membrane recruitment and LAT clustering in the presence or absence of CD45. LAT clustering was quantified as variance of fluorescence intensities measured by TIRF microscopy (see Methods). **(B)** Images of LAT clustering induced by TCR phosphorylation in the presence or absence of CD45. Scale bar: 2 μm. Experimental conditions were described in Fig. 3A.

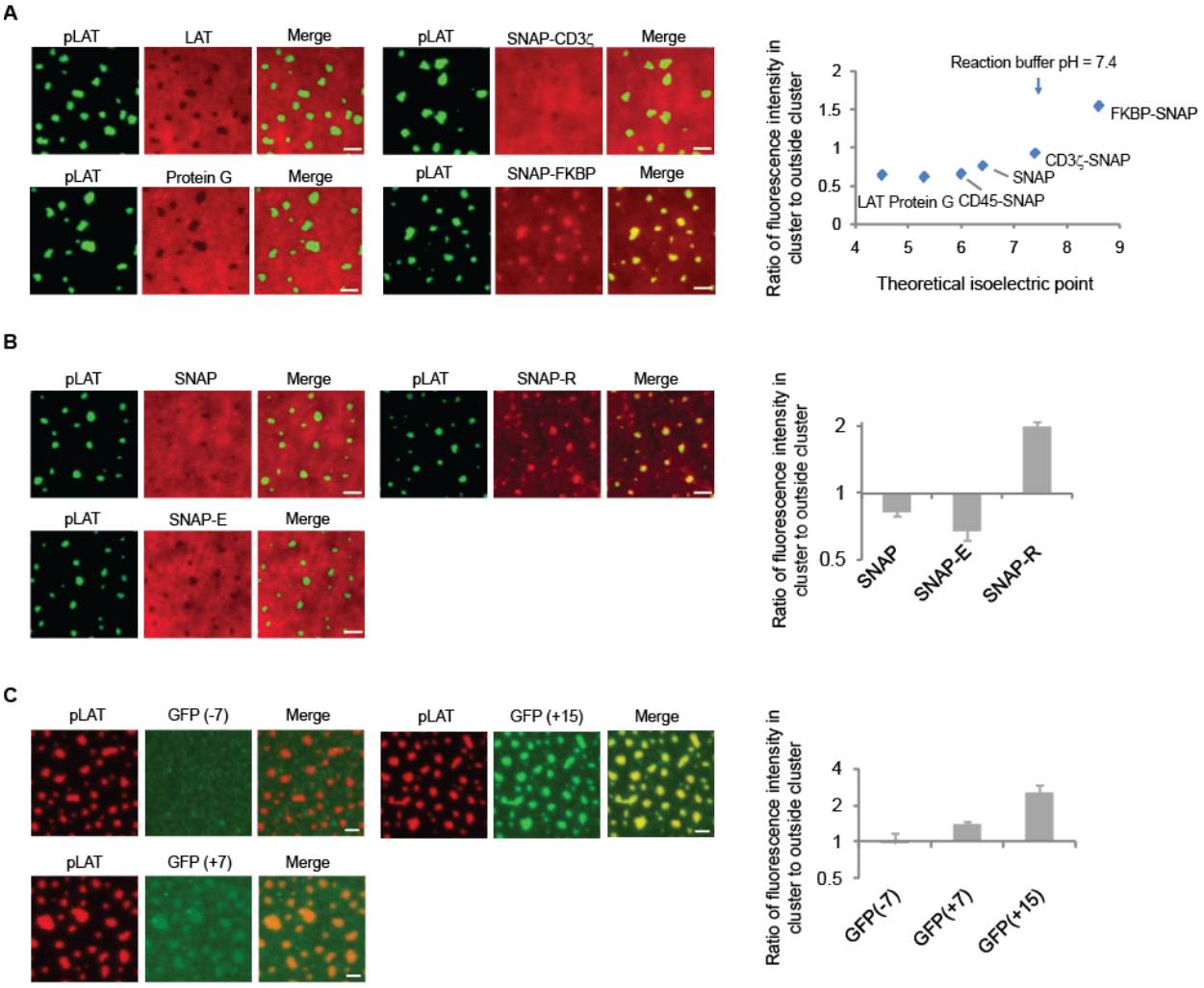

Fig. S7. LAT clusters exclude negatively-charged proteins but enrich positively charged proteins. (A) pLAT-Alexa488 (300 molecules/μm^2) bound to planar lipid bilayers was incubated with 1 μM Grb2 and 1 μM Sos1. Then 4 nM of His-tagged unphosphorylated LAT, Protein G (Fc binding domain), SNAP, unphosphorylated CD3ζ-SNAP, or FKBP-SNAP was added and imaged by TIRF microscopy. Scale bar: 2 μm. RIGHT: Quantification of exclusion level versus theoretical isoelectric point of indicated proteins. Each dot represents a mean of 17 clusters of similar sizes (0.8-1.1 μm in diameter). **(B)** Wild-type SNAP, SNAP fused with 9 glutamates (SNAP-E), or 9 arginines (SNAP-R) was incubated with pLAT clusters. The exclusion or enrichment is quantified by the ratio of fluorescent intensity in clusters to outside clusters. Shown are mean ± s.d. (N=17 clusters). **(C)** Wild-type GFP (charge of -7), GFP variant displaying 7 or 15 positive charge was incubated with pLAT clusters. The exclusion or enrichment was quantified by the ratio of fluorescent intensity in clusters to outside clusters. Shown are mean ± s.d. (N=3 independent experiments).

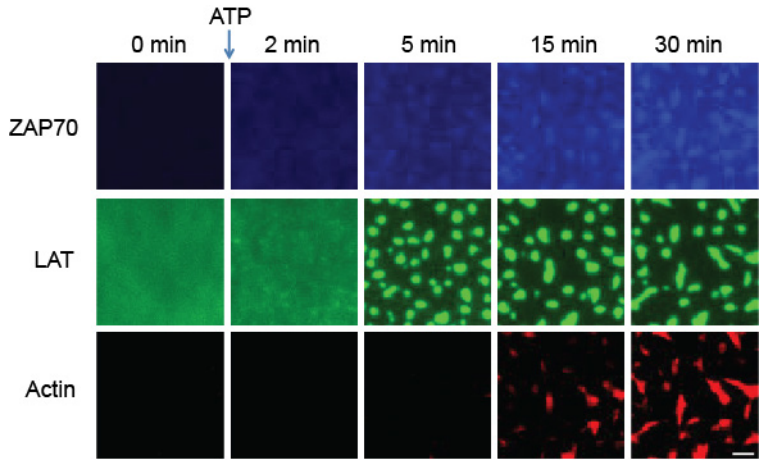

Fig. S8. Time courses of reconstituted TCR-LAT-actin signaling. TIRF microscopy revealed sequential membrane recruitment of ZAP70, LAT clustering, and actin polymerization in the reconstituted assay. The same experimental condition used in Fig. 4A was used here. Scale bar: 2 μm.

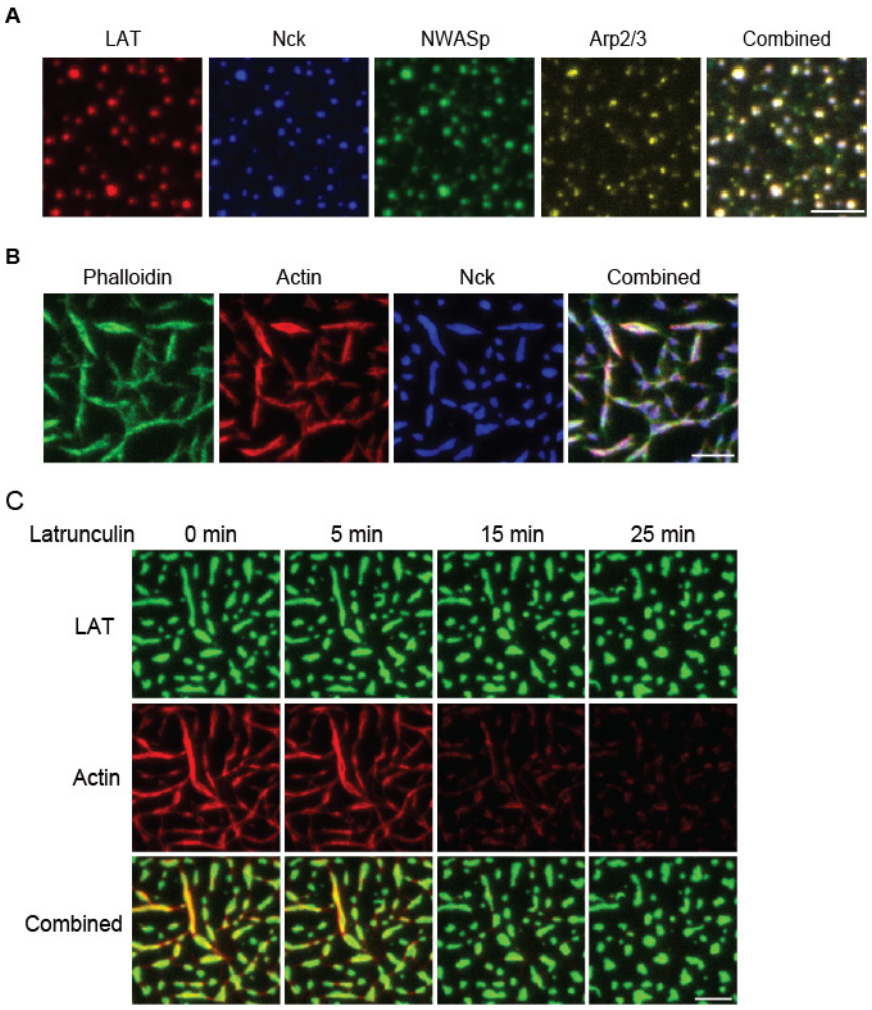

Fig. S9. Actin filaments change LAT cluster shape. (A) Actin regulators Nck, NWASp, and Arp2/3 were colocalized with LAT in clusters. The clusters displayed rounded shape in the absence of actin. **(B)** Phalloidin labeled actin structures assembled on LAT clusters. **(C)** Latrunculin was added to an assembled F-actin network with LAT clusters. F-actin was depolymerized which caused a morphological change of LAT clusters from rod-like to dot-like shape. Scale bar: 5 μm.

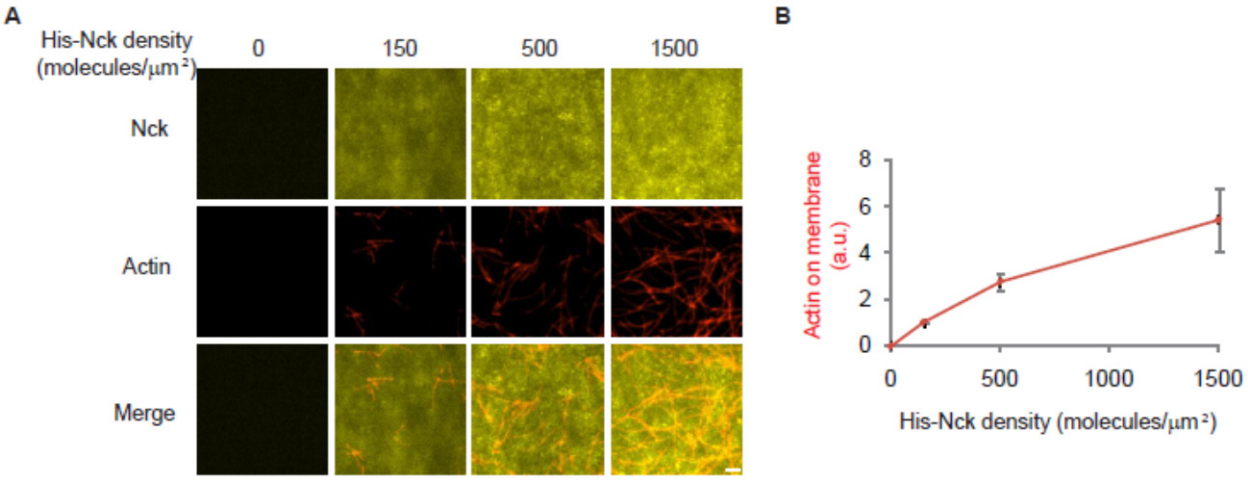

Fig. S10. Membrane-bound Nck promotes actin polymerization in a density-dependent manner. (A) TIRF microscopy images of His_{10}-Nck-Pacific Blue and actin-Rhodamine on the bilayer. Nck (0 - 1500 molecules/μm^2) was attached to the bilayer, and N-WASp (5 nM), Arp2/3 complex (0.25 nM), and actin (200 nM; 5% Rhodamine labeled) were in solution. 0.5 mM ATP-Mg was added to induce actin polymerization; images were recorded after 30 min. Scale bar: 2 μm. **(B)** Quantification of the actin fluorescence signal on the bilayer. Shown are mean $\pm$ s.e.m. (N=3 independent experiments).

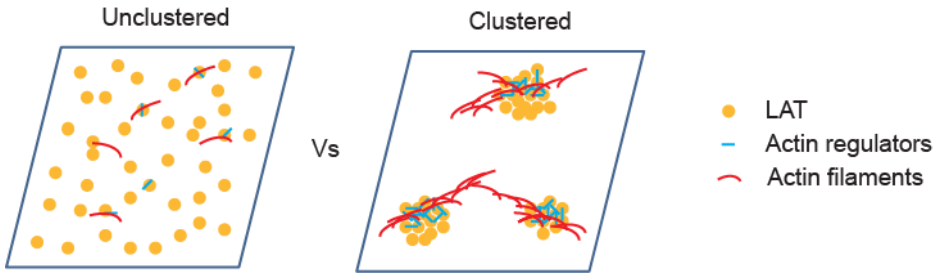

Fig. S11. A model for promoting actin polymerization by LAT clustering. When LAT is unclustered, actin regulators (Nck, N-WASp, and Arp2/3) are mostly in solution. Upon TCR triggering, LAT is phosphorylated and clustered. Clustered LAT recruit actin regulators to membranes, increases the local density as well as the membrane dwell time of these regulators, which promotes actin nucleation from the clusters.

Table S1. Sequences of constructs used in the study.

Construct	Sequence	Notes
CD3ζ	MGSSHHHHHHHHHHSSGLVPRGSHMA SMTGGQQMGRGSKKCKGSRVKFSRSA DAPAYQQGQNQLYNELNLGRREEYDV LDKRRGRDPEMGGKPQRRKNPQEGLY NELQKDKMAEAYSEIGMKGERRRGKG HDGLYQGLSTATKDTYDALHMQALPP R	Human cytoplasmic fragment, residues 52 - 164 , fused with an N-terminal His_{10} tag
CD3ζ-SNAP	MGSSHHHHHHHHHHGGGSGGGSGGG SRVKFSRSADAPAYQQGQNQLYNELN LGRREEYDVLDKRRGRDPEMGGKPQR RKNPQEGLYNELQKDKMAEAYSEIGM KGERRRGKGHDGLYQGLSTATKDTYD ALHMQALPPRGGSGGSDKDCEMKRTT LDSPLGKLELSGCEQGLHRIIFLGKGTS AADAVEVPAPAAVLGGPEPLMQATAW LNAYFHQPEAIEEFPVPALHHPVFQQES FTRQVLWKLLKVVKFGEVISYSHLAAL AGNPAATAAVKTALSGNPVPILIPCHR VVQGDLDVGGYEGGLAVKEWLLAHE GHRLGKPGLGGDSLEFIASKLA	Human cytoplasmic fragment, residues 52 - 164 , fused with an N-terminal His_{10} tag and C-terminal SNAP tag
CD45	MSYYHHHHHHHHHHDYDIPTTENLYF QGAMGSGIQRPTSTSSTRKIYDLHKKRS CNLDEQQELVERDDEKQLMNVEPIHA DILLETYKRKIADEGRLFLAEFQSIPRVF SKFPIKEARKPFNQNKNRYVDILPYDY NRVELSEINGDAGSNYINASYIDGFKEP RKYIAAQGPRDETVDDFWRMIWEQKA TVIVMVTRCEGNRNKCAEYWPSMEEG TRAFGDVVVKINQHKRCPDYIIQKLNIV NKKEKATGREVTHIQFTSWPDHGVPED PHLLLKLRRRVNAFSNFFSGPIVVHCSA GVGRTGTYIGIDAMLEGLEAENKVDV YGYVVKLRRQRCLMVQVEAQYILIHQ ALVEYNQFGETEVNLSELHPYLHNMK KRDPPSEPSPLEAEFQRLPSYRSWRTQH IGNQEENKSKNRNSNVIPYDYNRVPLK HELEMSKESEHDSDESSDDDSDSEEPS KYINASFIMSYWKPEVMIAAQGPLKETI GDFWQMIFQRKVKVIVMLTELKHGDQ EICAQYWGEGKQTYGDIEVDLKDTDK SSTYTLRVFELRHSKRKDSRTVYQYQY TNWSVEQLPAEPKELISMIQVVKQKLP	Human cytoplasmic fragment, residues 598 - 1304, fused with an N-terminal His_{10} and a C-terminal SNAP tag

	QKNSSEGNKHHKSTPLLIHCRDGSQQT GIFCALLNLLESAETEEVVDIFQVVKAL RKARPGMVSTEQYQFLYDVIASTYPAQ NGQVKKNNHQEDKIEFDNEVDKVKQD ANCVNPLGAPEKLPEAKEQAEGSEPTS GTEGPEHSVNGPASPALNQGSGSMDK DCEMKRTTLDSPLGKLELSGCEQGLHR IIFLGKGTSAADAVEVPAPAAVLGGPEP LMQATAWLNAYFHQPEAIEEFPVPALH HPVFQQESFTRQVLWKLLKVVKFGEVI SYSHLAALAGNPAATAAVKTALSGNP VPILIPCHRVVQGDLDVGGYEGGLAVK EWLLAHEGHRLGKPGLG	
FKBP-SNAP	MGSSHHHHHHHHHHSSGLVPRGSHMA SMTGGQQMGRGSGIQRPTSTSSTRGVQ VETISPGDGRTFPKRGQTCVVHYTGML EDGKKFDSSRDRNKPFKFMLGKQEVIR GWEEGVAQMSVGQRAKLTISPDYAYG ATGHPGIIPPHATLVFDVELLKLEGSGS GSGGGGSSTRMDKDCEMKRTTLDSPL GKLELSGCEQGLHEIKLLGKGTSAADA VEVPAPAAVLGGPEPLMQATAWLNAY FHQPEAIEEFPVPALHHPVFQQESFTRQ VLWKLLKVVKFGEVISYQQLAALAGN PAATAAVKTALSGNPVPILIPCHRVVSS SGAVGGYEGGLAVKEWLLAHEGHRLG KPGLGGSGSGSGGGGSSTS	FKBP fused with an N-terminal His_{10} tag
Gads	GPLGSEAVAKFDFTASGEDELSFHTGD VLKILSNQEEWFKAELGSQEGYVPKNF IDIQFKWFHEGLSRHQAENLLMGKEVG FFIIRASQSSPGDFSISVRHEDDVQHFKV MRDNKGNYFLWTEKFPSLNKLVDYYR TNSISRQKQIFLRDRTREDQGHEYKLIL NGKTLKGETTTEAVDAATAEKVFKQY ANDNGVDGEWTYDDATKTFTVTEHTD PVQLQAAGRVRWARALYDFEALEDDE LGFHSGEVVEVLDSSNPSWWTGRLHN KLGLFPANYVAPMTRC	Human, residues 1-155 and 261-330 fused with a GB1 domain in between. GB1 domain was included to increase the protein solubility. An additional Cys was added to the C-terminal for labeling.
GFP (-7, WT)	MGHHHHHHHHHHGENLYFQGSMVSK GEELFTGVVPILVELDGDVNGHKFSVS GEGEGDATYGKLTLKFICTTGKLPVPW PTLVTTLTYGVQCFSRYPDHMKQHDFF KSAMPEGYVQERTIFFKDDGNYKTRAE VKFEGDTLVNRIELKGIDFKEDGNILGH KLEYNYNSHNVYIMADKQKNGIKVNF KIRHNIEDGSVQLADHYQQNTPIGDGP	GFP fused with an N-terminal His_{10} tag

	VLLPDNHYLSTQSKLSKDPNEKRDHM VLLEFVTAAGITLGMDELYK	
GFP (+7)	MGHHHHHHGGASKGEELFTGVVPILV ELDGDVNGHKFSVRGEGEGDATNGKL TLKFICTTGKLPVPWPTLVTTLTYGVQ CFSRYPDHMKQHDFFKSAMPEGYVQE RTISFKDDGTYKTRAEVKFEGDTLVNRI ELKGIDFKEDGNILGHKLEYNFNSHNV YITADKRKNGIKAKFKIRHNVKDGSVQ LADHYQQNTPIGRGPVLLPRNHYLSTR SKLSKDPKEKRDHMVLLEFVTAAGIKH GRDERYK	GFP charge variant fused with an N-terminal His_6 tag
GFP (+15)	MGHHHHHHGGASKGERLFTGVVPILV ELDGDVNGHKFSVRGEGEGDATRGKL TLKFICTTGKLPVPWPTLVTTLTYGVQ CFSRYPKHMKRHDFFKSAMPEGYVQE RTISFKKDGTYKTRAEVKFEGRTLVNRI ELKGRDFKEKGNILGHKLEYNFNSHNV YITADKRKNGIKANFKIRHNVKDGSVQ LADHYQQNTPIGRGPVLLPRNHYLSTR SALSKDPKEKRDHMVLLEFVTAAGITH GMDELYK	GFP charge variant fused with an N-terminal His_6 tag
Grb2	GPLGSMEAIAKYDFKATADDELSFKRG DILKVLNEECDQNWYKAELNGKDGFIP KNYIEMKPHPWFFGKIPRAKAEEMLSK QRHDGAFLIRESESAPGDFSLSVKFGND VQHFKVLRDGAGKYFLWVVKFNSLNE LVDYHRSTSVSRNQQIFLRDIEQVPQQP TYVQALFDFDPQEDGELGFRRGDFIHV MDNSDPNWWKGACHGQTGMFPRNYV TPVNRNV	Human, residues 1 - 217.
Grb2ΔSH3	GPLGSMEAIAKYDFKATADDELSFKRG DILKVLNEECDQNWYKAELNGKDGFIP KNYIEMKPHPWFFGKIPRAKAEEMLSK QRHDGAFLIRESESAPGDFSLSVKFGND VQHFKVLRDGAGKYFLWVVKFNSLNE LVDYHRSTSVSRNQQIFLRDIEQV	Human, residues 1 - 154
Grb2-PreScission Cleavable	MEAIAKYDFKATADDELSFKRGDILKV LNEECDQNWYKAELNGKDGFIPKNYIE MKPHPWFFGKIPRAKAEEMLSKQRHD GAFLIRESESAPGDFSLSVKFGNDVQHF KVLRDGAGKYFLWVVKFNSLNELVDY HRSTSVSRNQQIFLRDIEQVPQQGGSLE VLFQGGSPTYVQALFDFDPQEDGELGF RRGDFIHVMDNSDPNWWKGACHGQT GMFPRNYVTPVNRNV	Human, residues 1 - 217. Inserted PreScission protease site between SH2 and C-terminal SH3 domains (Underlined)

LAT	HHHHHHHHGIQFKRPHTVAPWPPAFPP VTSFPPLSQPDLLPIPRSPQPLGGSHRTP SSRRDSDGANSVASFENEEPACEDADE DEDDFHNPGYLVVLPDSTPATSTAAPS APALSTPGIRDSAFSMESIDDYVNVPES GESAEASLDGSREYVNVSQELHPGAAK TEPAALSSQEAEEVEEEGAPDYENLQE LN	Human, residues 48-233 (short isoform) with His_8 N-terminal fusion. This construct only contains the four C-terminal Tyr residues (Y132, Y171, Y191, and Y226) that are sufficient for TCR signaling. The rest four N-terminal Tyr residues were mutated to Phe. Y171, Y191, and Y226 (in red) are the three tyrosines that are recognized by Grb2 when phosphorylated.
Lck	MSYYHHHHHHHHHHDYDIPTTENLYF QGAMGSGIQRPTSTSSTRACGCSSHPE DDWMENIDVCENCHYPIVPLDGKGTLL IRNGSEVRDPLVTYEGSNPPASPLQDNL VIALHSYEPSHDGDLGFEKGEQLRILEQ SGEWWKAQSLTTGQEGFIPFNFVAKAN SLEPEPWFFKNLSRKDAERQLLAPGNT HGSFLIRESESTAGSFSLSVRDFDQNQG EVVKHYKIRNLDNGGFYISPRITFPGLH ELVRHYTNASDGLCTRLSRPCQTQKPQ KPWWEDEWEVPRETLKLVERLGAGQF GEVWMGYYNGHTKVAVKSLKQGSMS PDAFLAEANLMKQLQHQRLVRLYAVV TQEPIYIITEYMENGSLVDFLKTPSGIKL TINKLLDMAAQIAEGMAFIEERNYIHR DLRAANILVSDTLSCKIADFGLARLIED NEYTAREGAKFPIKWTAPEAINYGTFTI KSDVWSFGILLTEIVTHGRIPYPGMTNP EVIQNLERGYRMVRPDNCPEELYQLM RLCWKERPEDRPTFDYLRSVLEDFFTA TEGQYQPQP	Human, residues 3 - 509 with His_{10} N-terminal fusion
Nck1	GHMAEEVVVVAKFDYVAQQEQELDIK KNERLWLLDDSKSWWRVRNSMNKTG FVPSNYVERKNSARKASIVKNLKDTLG IGKVKRKPSVPDSASPADDSFVDPGER LYDLNMPAYVKFNYMAEREDELSLIK GTKVIVMEKCSDGWWRGSYNGQVGW FPSNYVTEEGDSPLGDHVGSLSEKLAA VVNNLNTGQVLHVVQALYPFSSSNDEE LNFEKGDVMDVIEKPENDPEWWKCRK INGMVGLVPKNYVTVMQNNPLTSGLE PSPPQCDYIRPSLTGKFAGNPWYYGKV TRHQAEMALNERGHEGDFLIRDSESSP	Human, residues 1-377

	NDFSVSLKAQGKNKHFKVQLKETVYCI GQRKFSTMEELVEHYKKAPIFTSEQGE KLYLVKHLS	
Nck1 (His_{10}-tagged)	MSMAEEVVVVAKFDYVAQQEQELDIK KNERLWLLDDSKSWWRVRNSMNKTG FVPSNYVERKNSARKASIVKNLKDTLG IGKVKRKPSVPDSASPADDSFVDPGER LYDLNMPAYVKFNYMAEREDELSLIK GTKVIVMEKCSDGWWRGSYNGQVGW FPSNYVTEEGDSPLGDHVGSLSEKLAA VVNNLNTGQVLHVVQALYPFSSSNDEE LNFEKGDVMDVIEKPENDPEWWKCRK INGMVGLVPKNYVTVMQNNPLTSGLE PSPPQCDYIRPSLTGKFAGNPWYYGKV TRHQAEMALNERGHEGDFLIRDSESSP NDFSVSLKAQGKNKHFKVQLKETVYCI GQRKFSTMEELVEHYKKAPIFTSEQGE KLYLVKHLSLEGSENLYFQGAHHHHH HHHHH	Human, residues 1 - 377 with His_{10} C-terminal fusion
N-WASp	GSEFSPYDVPDYASGRGPNLPMATVDI KNPEITTNRFYSSQVNNISHTKEKKKGK AKKKRLTKADIGTPSNFQHIGHVGWDP NTGFDLNNLDPELKNLFDMCGISEAQL KDRETSKVIYDFIEKTGGVEAVKNELR RQAPPPPPSRGGPPPPPPPPHSSGPPPPP ARGRGAPPPPPSRAPTAAPPPPPSRPG VVVPPPPPNRMYPPPPPALPSSAPSGPPP PPPLSMAGSTAPPPPPPPPPPGPPPPPG LPSDGDHQVPASSGNKAALLDQIREGA QLKKVEQNSRPVSCSGRDALLDQIRQG IQLKSVSDGQESTPPTPAPTSGIVGALM EVMQKRSKAIHSSDEDEDDDDEEDFED DDEWEDC	Rat, residues 151 - 501 with an N-terminal HA tag and a C-terminal Cys for labeling
Protein G	MGSSHHHHHHHHHHGGGSGGGSGGG SGSGGTYKLILNGKTLKGETTTEAVDA ATAEKVFKQYANDNGVDGEWTYDDA TKTFTVTEKPEVIDASELTPAVTTYKLV INGKTLKGETTTEAVDAATAEKVFKQY ANDNGVDGEWTYDDATKTFTVTEKPE VIDASELTPAVTTYKLVINGKTLKGETT TKAVDAETAEKAFKQYANDNGVDGV WTYDDATKTFTVTEGCTLVSGRTRAPP PPPLRSGC	*Streptococcus,* Fc binding region, residues 309 - 497 with His_{10} N-terminal fusion
PTP1B	MEKEFEQIDKSGSWAAIYQDIRHEASD FPCRVAKLPKNKNRNRYRDVSPFDHSR IKLHQEDNDYINASLIKMEEAQRSYILT	Human, residues 3-277

	QGPLPNTCGHFWEMVWEQKSRGVVM LNRVMEKGSLKCAQYWPQKEEKEMIF EDTNLKLTLISEDIKSYYTVRQLELENL TTQETREILHFHYTTWPDFGVPESPASF LNFLFKVRESGSLSPEHGPVVVHCSAGI GRSGTFCLADTCLLLMDKRKDPSSVDI KKVLLEMRKFRMGLIQTADQLRFSYLA VIEG	
SLP-76	GHMDNGGWSSFEEDDYESPNDDQDGE DDGDYESPNEEEEAPVEDDADYEPPPS NDEEALQNSILPAKPFPNSNSMFIDRPP SGKTPQQPPVPPQRPMAALPPPPAGRN HSPLPPPQTNHEEPSRSRNHKTAKLPAP SIDRSTKPPLDRSLAPFDREPFTLGKKPP FSDKPSIPAGRSLGEHLPKIQKPPLPPTT ERHERSSPLPGKKPPVPKHGWGPDRRE NDEDDVHQRPLPQPALLPMSSNTFPSR STKPSPMNPLSSHMPGAFSESNSSFPQS ASLPPFFSQGPSNRPPIRAEGRNFPLPLP NKPRPPSPAEEENCSLNEGSLEVLFQ	Human, residues 101-420
SNAP (E/R)	MGSSHHHHHHHHHHGGGSGGGSGGG SDKDCEMKRTTLDSPLGKLELSGCEQG LHRIIFLGKGTSAADAVEVPAPAAVLG GPEPLMQATAWLNAYFHQPEAIEEFPV PALHHPVFQQESFTRQVLWKLLKVVKF GEVISYSHLAALAGNPAATAAVKTALS GNPVPILIPCHRVVQGDLDVGGYEGGL AVKEWLLAHEGHRLGKPGLGGDSLEFI ASKLA	SNAPf with an N-terminal His_{10} tag. SNAP-E contains an additional 9E on the C-terminus whereas SNAP-R contains an additional 9R on the C-terminus.
Sos1	GPLGSNDTVFIQVTLPHGPRSASVSSISL TKGTDEVPVPPPVPPRRRPESAPAESSP SKIMSKHLDSPPAIPPRQPTSKAYSPRY SISDRTSISDPPESPLLPPREPVRTPDVFS SSPLHLQPPPLGKKSDHGNAFFPNSPSP FTPPPPQTPSPHGTRRHLPSPPLTQEVDL HSIAGPPVPPRQSTSQHIPKLPPKTYKRE HTHPSMC	Human, poly-proline rich region, residues 1117-1319 with a Cys added at the C-terminus for labeling
ZAP70	GPTRMDKDCEMKRTTLDSPLGKLELSG CEQGLHEIKLLGKGTSAADAVEVPAPA AVLGGPEPLMQATAWLNAYFHQPEAI EEFPVPALHHPVFQQESFTRQVLWKLL KVVKFGEVISYQQLAALAGNPAATAA VKTALSGNPVPILIPCHRVVSSSGAVGG YEGGLAVKEWLLAHEGHRLGKPGLGG SGSGSGGGGSSTRMPDPAAHLPFFYGSI SRAEAEEHLKLAGMADGLFLLRQCLRS	Human, residues 1 - 619 fused with an N-terminal SNAP tag

	LGGYVLSLVHDVRFHHFIERQLNGTYA IAGGKAHCGPAELCEFYSRDPDGLPCN LRKPCNRPSGLEPQPGVFDCLRDAMVR DYVRQTWKLEGEALEQAIISQAPQVEK LIATTAHERMPWYHSSLTREEAERKLY SGAQTDGKFLLRPRKEQGTYALSLIYG KTVYHYLISQDKAGKYCIPEGTKFDTL WQLVEYLKLKADGLIYCLKEACPNSSA SNASGAAAPTLPAHPSTLTHPQRRIDTL NSDGYTPEPARITSPDKPRPMPMDTSV YESPYSDPEELKDKKLFLKRDNLLIADI ELGCGNFGSVRQGVYRMRKKQIDVAI KVLKQGTEKADTEEMMREAQIMHQLD NPYIVRLIGVCQAEALMLVMEMAGGG PLHKFLVGKREEIPVSNVAELLHQVSM GMKYLEEKNFVHRDLAARNVLLVNRH YAKISDFGLSKALGADDSYYTARSAGK WPLKWYAPECINFRKFSSRSDVWSYG VTMWEALSYGQKPYKKMKGPEVMAFI EQGKRMEPPECPPELYALMSDCWIYK WEDRPDFLTVEQRMRACYYSLASKVE GPPGSTQKAEAACA	

Table S2. Physical properties of LAT clusters

	Size	Roundness	Half recover time
Minimal components (LAT, Grb2, and Sos1)	0.39 ± 0.02 μm^2 (N=277)	0.79 ± 0.11 (N=277)	76 ± 12 sec (N=7)
Full pathway (TCR-LAT-actin)	0.82 ± 0.03 μm^2 (N=301)	0.51 ± 0.21 (N=301)	98 ± 37 sec (N=10)

Shown are mean $\pm$ S.E. for size, mean $\pm$ S.D. for roundness and half recover time. N indicates the number of clusters quantified.

Movie S1. Single molecule imaging of pLAT on supported lipid bilayers. His_8-pLAT-Cy3B was attached to Ni-functionalized lipid bilayers at ~0.15 molecules/μm^2. pLAT mobility was revealed by TIRF imaging. Shown is a field view of 20 μm x 20 μm. The movie is played at 20 fps with a frame interval of 30 ms.

Movie S2. Assembly and disassembly of LAT clusters. His_8-pLAT-Alexa488 was attached to Ni-functionalized lipid bilayers at 1000 molecules/μm^2. Clusters were formed after Grb2 (0.5 μM) and Sos1(0.25 μM) was added at 0 min. Protein tyrosine phosphatase PTP1B (2 μM) was added at time 9 min and disassembled clusters. Shown is a field view of 24 μm x 24 μm. The movie is played at 20 fps with a frame interval of 5 s.

Movie S3. Single molecule imaging of a single pLAT molecule (red) trapped by a cluster (green), released, and re-trapped by another cluster. pLAT-Alexa488 (300 molecules/μm^2) was incubated with Grb2 (0.5 μM) and Sos1 (0.25 μM). pLAT-TMR was included at 0.07 molecules/μm^2. To generate this movie, a single image of pLAT-Alexa488 (to indicate cluster position) was superimposed onto a timelapse video recording pLAT-TMR movement. Shown is a field view of 6 μm x 6 μm. The movie is played at 10 fps with a frame interval of 50 ms.

Movie S4. Reconstitution of a TCR-LAT-actin pathway. TIRF microscopy revealed LAT clustering (blue) followed by actin polymerization (red) on supported lipid bilayers. The same condition was used as in Fig. 3D. ATP was added at 2:00. Shown is a field view of 24 μm x 24 μm. The movie is played at 10 fps with a frame interval of 1 min.

Movie S5. Reconstitution of a TCR-LAT-actin pathway in the absence of actin. TIRF microscopy revealed LAT clustering (blue) on supported lipid bilayers. Note that in contrast to Video 4, LAT clusters did not elongate in the absence of actin. The same condition was used as in Fig. 3D except actin was omitted. ATP was added at 2:00. Shown is a field view of 24 μm x 24 μm. The movie is played at 10 fps with a frame interval of 1 min.

Author Contributions

X.S., J.A.D., M.K.R., and R.D.V. conceived of the project and designed the experiments. J.A.D., X.S., E.H., W.X., S.B., and J.O. prepared the reagents. X.S. and J.A.D. performed the experiments of LAT cluster formation with different adaptors and disassembly with PTP1B. X.S. performed the experiments of pLAT density titration, measurement of LAT mobility, LAT cluster exclusion (except GFP), CD45 dephosphorylation activity, LAT clustering kinetics with different adaptors, TCR to actin signaling reconstitution, actin polymerization induced by Nck clustering, and cellular experiments on LAT clustering and ERK activation. J.A.D. performed the experiments of LAT cluster formation with tyrosine mutants in vitro, protease-induced LAT declustering, and LAT cluster exclusion of GFP charge mutants. W.X. performed the experiments of phase diagrams of LAT and tyrosine mutants. X.S., J.A.D., M.K.R., and R.D.V. wrote the manuscript with input from J.T.

References

28. Y. D. Chung, M. D. Sinzinger, P. Bovee-Geurts, M. Krause, S. Dinkla, I. Joosten, W. J. Koopman, M. J. Adjobo-Hermans, R. Brock, Analyzing the homeostasis of signaling proteins by a combination of Western blot and fluorescence correlation spectroscopy. *Biophysical journal* **101**, 2807-2815 (2011).
29. B. F. Lillemeier, M. A. Mortelmaier, M. B. Forstner, J. B. Huppa, J. T. Groves, M. M. Davis, TCR and Lat are expressed on separate protein islands on T cell membranes and concatenate during activation. *Nature immunology* **11**, 90-96 (2010).
30. E. Sherman, V. Barr, S. Manley, G. Patterson, L. Balagopalan, I. Akpan, C. K. Regan, R. K. Merrill, C. L. Sommers, J. Lippincott-Schwartz, L. E. Samelson, Functional nanoscale

organization of signaling molecules downstream of the T cell antigen receptor. *Immunity* **35**, 705-720 (2011).
31. D. J. Williamson, D. M. Owen, J. Rossy, A. Magenau, M. Wehrmann, J. J. Gooding, K. Gaus, Pre-existing clusters of the adaptor Lat do not participate in early T cell signaling events. *Nature immunology* **12**, 655-662 (2011).
32. S. J. Davis, P. A. van der Merwe, The kinetic-segregation model: TCR triggering and beyond. *Nature immunology* **7**, 803-809 (2006).